MEASUREMENT AND MODELING OF THERMAL PROPERTIES OF COARSE-GRAINED SOILS

By

Jun Yao

A thesis submitted in partial fulfillment of the requirements for the degree of

MASTER OF SCIENCE
(GEOLOGICAL ENGINEERING)

At the
UINVERSITY OF WISCONSIN-MADISON
2014

MEASUREMENT AND MODELING OF THERMAL PROPERTIES OF COARSE-GRAINED SOILS

Student Name **Campus ID Number**

Approved

Date

William J. Likos

Associate Professor

EXECUTIVE SUMMARY

The purpose of this study is to experimentally determine and mathematically represent the thermal resistivity or thermal conductivity dry-out curves (TRDCs or TCDCs) quantifying the relation between thermal resistivity or thermal conductivity and pore water saturation for coarse-grained soils (sands). TRDCs or TCDCs were measured for thirteen sandy soils representing a range of grain characteristics and grain-size distribution. Experiments were conducted using three laboratory methods for comparison, including: (i) a modified hanging column apparatus instrumented for concurrent measurement of the TRDC and soil-water characteristic curve (SWCC), (ii) a staged-drying method involving use of remolded cylindrical specimens subjected to discrete drying increments, and (iii) a multiple-specimen method involving preparation of several identical specimens at different water contents for independent thermal resistivity measurements. Quantitative comparison of resulting TRDCs and error analyses were performed. The modified hanging column method produces the most robust and well-defined TRDCs, but potential overestimation of thermal resistivity may occur during initial drainage, possibly due to forced convection caused by water movement and free convection caused by a larger heat pulse created by the SH-1 (dual needle) thermal probe. The staged-drying and multiple-specimen methods have an advantage of relatively rapid testing time. Producing TRDCs using these methods required 10 days and 1 day, respectively, whereas the hanging column method required an average of 23 days. Analysis of variability shows that observed measurement scatter for the staged-drying and multiple-specimen methods are likely attributed to sample heterogeneity. Based on observations of the measured TCDCs, two new mathematical models were developed for modeling the thermal conductivity of unsaturated coarse-grained soils at room temperature. The models are based on observations of four different regimes in

measured TCDCs. Correlations between the model parameters and soil physical parameters are examined. Modeled TCDCs are shown to provide good match with measured TCDCs. Averaged coefficients of determination are 0.957 and 0.974 for the two different models, demonstrating that they may provide better predictions than many previous models for coarse-grained soils.

ACKNOWLEDGEMENTS

I would like to especially thank my advisor, Professor William J. Likos, for his invaluable advice and endless support during my graduate studies. Thank you for your great mentorship and guidance. I would also like to express my thanks to my thesis committee members, Professors James Tinjum and Dante Fratta. Thank you for providing opinions and suggestions for the improvement of my knowledge and experience. Additionally, I would like to thank my research group colleagues Hyunjun Oh and Ray Wu for their help and support for the laboratory work and research. Also, I sincerely thank Xiaodong Wang, the geotechnical laboratory manager, for his great support and assistance in the laboratory.

I am extremely grateful to my parents for providing constant source of support not only for my graduate study but also during all my life. I would also like to thank to my friends, and especially all my geo-friends for their support and keeping geo-community in very joyful environment.

This material is based upon work supported by the National Science Foundation (NSF) under Grant CMMI 0968768. Any opinions, findings, and conclusions or recommendations expressed in this material are those of the authors and do not necessarily reflect the views of NSF.

TABLE OF CONTENTS

LIST OF FIGURES

LIST OF TABLES

CHAPTER ONE

INTRODUCTION

In recent years, thermally-active ground structures, such as ground-source heat pumps, have been increasingly developed due to the increasing need for various types of energy resources, especially for environmentally-friendly energy. Soil thermal properties, such as thermal conductivity, play important roles in this type of thermal-active ground structure. Incomplete understanding of soil thermal properties (e.g., overestimation of thermal conductivity of surrounding soils) could result in less efficient and economical design of thermal-active structures.

In this study, the relationships between thermal resistivity or thermal conductivity and pore water saturation were investigated. The study focuses on comparing laboratory methods for measuring thermal resistivity dry-out curves (TRDCs) and developing new models for predicting thermal conductivity dry-out curves (TCDCs) of coarse-grained, granular soils (sands) at room temperature. Chapter 2 investigates differences between three laboratory testing methods for obtaining TRDCs on coarse-grained soils, including a multiple-specimen method, a staged-drying method, a modified hanging column method. These three different methods were compared quantitatively by determining the difference in thermal resistivity measurements at the same degree of saturation for the three methods. Chapter 3 introduces two new mathematical models for modeling and predicting TCDCs. The new models were compared to a suite of existing models for predicting TCDCs available in the literature. Chapter 4 summarizes conclusions drawn from Chapter 2 and Chapter 3, and makes recommendations for future work. Finally, Chapter 5 is an appendix that is included to document a related study regarding the

effects of constraints on van Genuchten (VG) parameters for modeling soil-water characteristic curves (SWCCs).

CHAPTER TWO

COMPARISON OF LABORATORY METHODS FOR PRODUCING THERMAL RESISTIVITY DRY-OUT CURVES OF COARSE-GRAINED SOILS

2.1 INTRODUCTION

Soil thermal properties, especially thermal conductivity (λ) or thermal resistivity (ρ), are important for many engineering applications. Examples of such engineering applications include underground storage systems, estimation of frost heave and thaw settlement in cold regions, municipal solid waste landfill and backfill design for buried pipelines (Shelton, 1975; Guymon *et al.*, 1993; Southen and Rowe, 2005; Li *et al.*, 2013). More recent applications include backfill design for buried power cables and shallow geothermal heat exchangers. Heat generated from electrical losses in buried cables must transfer effectively through the backfill to maintain efficiency of the power cables and a safe cable operating temperature (Brandon *et al.*, 1989; Freitas and Prata, 1996; Gouda *et al.*, 2011). If the backfill has high thermal resistivity, the heat cannot effectively dissipate and can lead to cable overheating or failure. Efficiency of heat transfer in geothermal systems is directly dependent on the thermal characteristics of surrounding soil or rock and the changes in these characteristics as affected by the environment (e.g., precipitation and evaporation). Historical and ongoing research on soil thermal properties and heat transport in saturated and unsaturated soils has been driven by these and other emerging applications (e.g., Donazzi *et al.*, 1979; Dayan and Merbaum, 1984; Fan *et al.*, 2007; Woodward and Tinjum, 2012).

In near ground surface applications, the soils are often unsaturated and include multiple phases (i.e. solid, liquid and gas). Since heat flows through these three phases with different resistance, the bulk or effective thermal resistivity of porous media is significantly dependent on

the degree of pore water saturation. According to Kersten (1949), the thermal resistivity of typical soil solids, water, and air are about 4 ºC-cm/W, 165 ºC-cm/W, and 4000 ºC-cm/W, respectively. Thermal resistivity dry-out curves (TRDCs) quantify the non-linear relationship between effective thermal resistivity (ρ) and degree of pore water saturation (S). Thermal resistivity is generally at a minimum for fully saturated conditions, increases with decreasing saturation, dramatically increases at some critical saturation, and ultimately reaches some maximum at zero saturation (Smits *et al.*, 2010; Likos *et al.*, 2012; Woodward and Tinjum, 2012; Likos, 2013). Increasing resistivity with decreasing saturation reflects the presence of the less conductive air-phase in the multiphase unsaturated soil system.

Farouki (1981) provides a comprehensive review of soil thermal properties, summarizes major factors that influence heat transfer processes in soil, and gives an overview of many of the experimental and modeling methods available for quantifying soil thermal behavior and the TRDC. ASTM International test standard ASTM D5334-08 and Institute of Electrical and Electronics test standard IEEE 442-1981 describe procedures for obtaining soil thermal resistivity or thermal conductivity measurements using transient thermal probe methods. While no specific approach has yet to have been standardized for measuring the TRDC, several laboratory testing methods have been developed and applied along drying and wetting paths. These most notably include the *multiple-specimen* method (Campbell, 2011; Likos *et al*., 2012), the *staged-drying* method (Woodward and Tinjum, 2012), and instrumented Tempe cell or hanging column methods (e.g., Smits *et al.*, 2010; Likos *et al.*, 2012). Woodward and Tinjum (2012) and Likos *et al.* (2012) report results from experiments designed to examine influences of issues inherent to each approach, including gravity-induced moisture migration, drying temperature, drying time, sensor location, sensor orientation, and sample heterogeneity. A

variety of approaches for modeling or estimating the TRDC have also been proposed, most of which are based on empirical correlation to more easily measured soil properties (e.g. Farouki, 1981; Campbell, 1985; Côté and Konrad, 2005).

The purpose of this study is to investigate the differences between three laboratory testing methods for obtaining TRDCs on coarse-grained soils, including the multiple-specimen method, the staged-drying method, and modified hanging column method. These three different methods were compared quantitatively by determining the difference in thermal resistivity measurements at the same degree of saturation for the three methods.

2.2 MATERIALS AND METHODS

2.2.1 Test Materials

Twelve sandy soils were selected to evaluate the laboratory methods for producing TRDCs (Table 2-1). These soils included: (*i*) eight sandy soils from the University of Wisconsin-Madison Soil Bank, which contains a total of 30 sands collected from various geological deposits in Wisconsin (Bareither *et al.*, 2008), (ii) three artificially created well-graded sands, and (iii) a sandy soil from Grand Marsh, Wisconsin. Figure 2-1 shows grain-size distribution (GSD) curves for the 12 soils obtained using mechanical sieve analysis (ASTM D422). Two additional hydrometer tests were performed on two soils (SM1 and SM2) to successfully capture the D_{10} from the GSD curves. For those soils with more than 5% fines, the portions passing the No.40 sieve were sampled for plastic limit and liquid limit tests (ASTM D4318).

According to the Unified Soil Classification System (USCS) based on the ASTM D2487, results from mechanical sieve analysis, hydrometer tests, plastic limit and liquid limit tests were used to classify the 12 materials into 5 soil types: (*i*) Poorly Graded Sand, SP; (*ii*) Well-Graded

Sand, SW; (*iii*) Silty Sand, SM; (*iv*) Poorly Graded Sand with Silt, SP-SM; and (*v*) Well-Graded Sand with Silt, SW-SM. Table 2-1 summarizes the test material properties including D_{50}, D_{10}, coefficient of uniformity (C_u), coefficient of curvature (C_c), fines content, specific gravity of the solids (G_s), minimum void ratio (e_{min}), maximum void ratio (e_{max}), roundness and sphericity. D_{50}, D_{10}, C_u and C_c and fines content were determined from the GSDs. The specific gravity was determined using ASTM D854. The minimum and maximum void ratios were obtained by ASTM D4254.

2.2.2 Modified Hanging Column Procedures

Soil-water characteristic curves (SWCCs) and TRDCs were obtained concurrently along an initial drying path (*i.e.*, drainage from $S = 1$) using an instrumented hanging column apparatus (Smits *et al.*, 2010; Likos *et al.*, 2012). The apparatus (Figure 2-2) consists of an acrylic confining sleeve, a perforated bottom plate, and a top cap. The bottom plate includes a brass screen designed to support a high-air-entry nylon membrane (diameter = 142 mm, pore size = 0.2 μm, air-entry pressure = 340 kPa), through which suction is applied to the sand via a hanging-column water system (ASTM D6836-02).

Sensors were directly buried in the sand to obtain measurements of suction, moisture content, temperature, and thermal resistivity/conductivity as suction was increased or decreased using the hanging water column. Measurements were interpreted to produce a continuous SWCC and TRDC along either a continuous drying or wetting path. The sensor for measuring matric suction (denoted I in Figure 2-2) is a small-tip tensiometer inserted through a plastic fitting on the side wall of the cell, embedded into the soil, and connected to a differential pressure transducer (Model P55D, Validyne Engineering Corp., Northridge, CA) and data-logger system.

The thermal sensor (II) is a dual-needle transient thermal probe (SH-1) connected to a KD2Pro data-acquisition system (Decagon Devices, Pullman, WA) for measuring soil thermal properties. The moisture sensor (III) is a dual-prong dielectric moisture sensor (ECH_2O EC-5, Decagon Devices, Pullman, WA) connected to an Decagon Em50 data logger. Raw data acquired from the moisture sensor was independently calibrated for each test material using the two-point α-mixing model from Sakaki *et al.* (2008). The temperature sensor (IV) was embedded into the top portion of the soil and connected to the Em50 data logger.

For the tests reported herein, sands were compacted to a void ratio (*e*) of 0.6. Dry sand, which was dried in an oven at 105 °C for 24 h, was compacted directly into the confining sleeve in four equal layers to a height of about 1 cm below the top edge of the cell. This resulted in a typical specimen height of 6.6 cm. The tensiometer, moisture sensor, and SH-1 sensor were embedded in the sand between the 2^{nd} and the 3^{rd} layers. Sakaki *et al.* (2008) conducted experiments to show that the bulk sampling volume of the EC-5 moisture sensor is approximately 18 cm^3, comprising 2 cm (parallel to prongs) × 1 cm (perpendicular to prongs) × 9 cm (longitudinal including sensor head). Thus, for a horizontally oriented moisture sensor, the water content measurement represents some average of the material 1 cm above and below the sensor. Thus the water content measurement obtained in the present apparatus is representative of a vertical region of sand equal to about 30% of the overall specimen height. The temperature sensor was inserted through a vent in the top cap and buried in the top portion of the sand after compaction.

After packing, valve 1 (Figure 2-2) was opened to wet the membrane and the specimen from bottom to top until approximately 1 cm water ponded on the top of the sand surface. The water level in the cell and standpipe was then brought down to the midpoint of the cell at the

elevation where the tensiometer, moisture sensor, and thermal probe were located. Valve 2 was then partially opened to produce a slow drip from the water column at a rate of 6 to 10 s/drip, thereby slowly and continuously increasing the suction head applied to the sand. After the water in the standpipe was completely drained at a suction head of ~126.5 cm H_2O, the top cap of the confining sleeve was removed, and a small mechanical fan was set up near the top of the specimen for continued drying through evaporation. Matric suction, volumetric water content, and thermal resistivity were continuously monitored until the volumetric water content of the sand reached a value less than about 0.01.

2.2.3 Multiple-Specimen Procedures

TRDCs measured using the instrumented hanging column were compared with independent measurements obtained using a multiple-specimen approach (e.g., Woodward and Tinjum, 2012; Likos *et al*., 2012). These tests were performed by direct measurement of thermal resistivity using a thermal needle probe inserted into multiple sand specimens compacted to target void ratio of 0.6 and over a range of water contents. Thermal resistivity for the dry sands was first measured by inserting a 10-cm-long, single-needle probe (TR-1, Decagon Devices, Inc.) into the top center of the compacted sand (vertical probe orientation). The dry sand was then poured into a large container, thoroughly mixed with an amount of water to produce target water content, and then re-compacted into the mold for a second thermal resistivity measurement. This was repeated for a total of 12 compacted specimens having 11 water content increments. Water content corresponding to each increment was determined after each test by sampling sand from the vicinity of the TR-1 probe for gravimetric measurement.

2.2.4 Staged-Drying Procedures

For the tests herein, the staged-drying method described by Woodward and Tinjum (2012) to investigate water redistribution during measurement of TRDCs was modified to obtain more consistent void ratios and more complete TRDCs. The required amount of water to achieve full saturation (S=1) for each layer was first filled into a chlorinated polyvinyl chloride (CPVC) cylinder (Figure 2-3) before the soil was poured into the water through a plastic funnel to avoid over-compacting the specimen. This was done with three equal lifts to achieve the target void ratio of 0.6. Four identical specimens were prepared for thermal resistivity measurements after 1 day, 3 days, 7 days and 10 days of oven drying at 50 °C. The purpose of this process is to improve the completeness of TRDCs by increasing the number of thermal resistivity measurements, especially for those near the knee point at low saturation where ρ dramatically increases. The TR-1 sensor was employed to measure the thermal resistivity by inserting it horizontally into the top, middle, and bottom locations of the specimen (Figure 2-3).At day zero, all four specimens were weighed and measured with the TR-1 sensor for thermal resistivity at S=1 from top to bottom. After each oven-drying period, one specimen was removed from the oven. Specimen weight and thermal resistivity at each location were measured after the specimen was cooled down for at least 2 hours. Samples were collected to determine gravimetric water content near all three sensor locations from top to bottom layers.

2.2.5 Variability Test Procedures

Likos *et al.* (2012) tested the variability resulting from spatial sample inhomogeneity and instrument scatter through two separate series of tests. In the first series, a large plastic tray was filled with dry sand covered by plastic wrap. A 20 cm × 12 cm grid with 4-cm grid spacing was

drawn on the plastic wrap to establish 24 measurement locations as shown in Figure 2-4. At each location, the TR-1 sensor was inserted vertically to obtain a measure of thermal conductivity variability. For further discussion, the results of this series were adopted to simulate the potential variability of ρ variability for the multiple-specimen and staged-drying methods. In the second series, the TR-1 sensor was inserted into the same location to obtain 24 consecutive measurements of thermal conductivity at 1-hr intervals. The purpose of the second series was to test the potential variability related to the single specimen test, which was not used in this study. Therefore, the second series was modified into the test related to the modified hanging column method. The SH-1 sensor was embedded into the dry sand between the 2^{nd} and the 3^{rd} layers of the acrylic container in the modified hanging column method. The sand used in this series is poorly graded sand (SP4), which is a different soil from the first series. The ρ measurements were obtained for 24 h at 15-min interval. Thus, potential variability associated to the SH-1 sensor in the modified hanging column method could be simulated.

2.3 RESULTS AND DISCUSSION

Figure 2-5 shows TRDCs obtained using modified hanging column, multiple-specimen, and staged-drying methods for three representative sands (SP5, SM2, SW-SM2). Each curve displays characteristics similar to those observed for coarse-grained soils in previous studies, such as Smits *et al.* (2010), Likos *et al.* (2012), and Woodward and Tinjum (2012). At the beginning of each curve, thermal resistivity (ρ) remains relatively constant, which indicates that the soils are effectively saturated but not fully saturated. The air, existing as small occluded bubbles in the pores, has a minimal effect on the heat transfer; thus, the heat largely migrates through saturated grain-water-grain pathways (Smits *et al.*, 2009). In this regime, the lower

bound of saturation varies from about 0.6 to 0.9 for all 12 sandy soils. As the degree of saturation decreases beyond this regime, the water phase is still continuous but more water is displaced by air, thus causing the heat to be forced to transfer through longer and fewer grain-water-grain pathways. This results in ρ increasing slowly in a generally linear trend until TRDC reaches the critical saturation (S_{crit}), where ρ starts to increase dramatically. After S drops below S_{crit}, the water forms isolated liquid bridges between grains, and diminishes through evaporation. Therefore, the heat transport becomes less effective through this weaker and more tortuous grain-water-grain pathway. Additionally, the reduction of water vapor in the pores could lead to the reduction of latent heat transport, which could also distribute to the dramatic increase of ρ (Campbell *et al.*, 1994). At the fully dried conditions, ρ is the highest because the conductive heat transport occurs primarily through the contacts between grains. Since the surfaces of the grains are not smooth, the contact resistance between grains is considered as a big factor on the dry ρ (Farouki, 1981).

TRDCs measured using the three different methods are comparable (Figure 2-5). However, the thermal resistivity for $S>S_{crit}$ measured using the modified hanging column can be as much as about 10% higher than the other two methods. The critical saturation (S_{crit}) was determined as the intersection of the extended lines extrapolated from two linear portions of TRDC. This phenomenon is consistent for all 12 sandy soils. Figure 2-6 shows the comparison of ρ values at the same degree of saturation for the three different methods. Figure 2-6(a) compares results from the staged drying and modified hanging column methods. Open symbols denote ρ measured at saturation below critical saturation (i.e. relative dry sand). Closed symbols denote ρ measured at saturation above critical saturation (i.e. relative moist sands). Figure 2-6(b) is a similar comparison between the multiple-specimen and modified hanging column methods.

From Figure 2-6(a), most of the ρ values for $S>S_{crit}$ fall into the zone above 1:1 line, and cluster around 1.1:1 line. This indicates that ρ values for $S>S_{crit}$ from the modified hanging column method are approximately 10% higher than those from staged-drying method. The reasons for this minro difference are not entirely clear, but may reflect water flow at high saturation. Higher ρ for $S>S_{crit}$ in the modified hanging column test is potentially attributed to forced convection caused by water flow during the measurement. This water flow is caused by the hydraulic gradient created from the hanging column. Moreover, the SH-1 sensor emits larger heat pulse than the TR-1 sensor resulting in larger free convection between the water and the sensor (Decagon Devices, 2014). Thus, both the forced and free convections may cause less accurate measurements in modified hanging column method when $S>S_{crit}$. However, the ρ values compared between modified hanging column and multiple-specimen method do not show significant difference for $S>S_{crit}$ in Figure 2-6(b). The data points are evenly distributed around 1:1 line for $S>S_{crit}$. This is likely due to the worse contact performance of the vertically inserted TR-1 sensor in multiple-specimen test than the horizontally inserted TR-1 sensor in staged-drying test. Especially for the highly saturated soils, the soils behave like a liquid, and the soil particles fail to contact well with the vertically inserted sensor. In contrast, the horizontally inserted sensor can perform better contact with wet soils because of gravity.

For $S<S_{crit}$, most ρ values fall below 1:1 line for both comparisons, which indicates that ρ values from staged-drying and multiple-specimen methods are higher than those from modified hanging column method. This is attributed to the different ways of placement of thermal probe. In the modified hanging column method, the SH-1 sensor was continuously in contact with soils throughout test. As the soil becomes dryer and dryer after $S<S_{crit}$, the fine particles could cement around the SH-1 sensor. In contrast, the TR-1 sensor was inserted into the specimen afterwards

in staged-drying and multiple-specimen tests. Thus, the contact resistance between the sensor and the specimen and disturbance from repeated probe insertion may have greater effects on ρ values in staged-drying and multiple-specimen methods than modified hanging column method.

Figure 2-7 displays errors output from KD2Pro analyzer changing with degree of saturation in three methods for SP5 and SP7. Error value produced from KD2Pro analyzer is a measure of how accurately the model built in analyzer fits the data collected from the sensor, and a data set with error value below 1% is often considered as a good data set (Decagon Devices, 2014). Figure 2-7(a) shows the error ranges from1.5% to 2.0% before some saturation (S~0.1) in modified hanging column method for SP5. This saturation is in general accordance with the critical saturation (S_{crit}). After critical saturation, the error decreases and reaches minimum (~0.4%) when soil is fully dried (S=0). Measurements with larger error before critical saturation is possibly due to the forced convection caused by water flow and the free convection caused by larger heat pulse emitted by SH-1 sensor. In contrary, since the potential bad contact may occur between inserted TR-1 sensor and dry soil particles, the staged-drying and multiple-specimen methods show relative greater error after critical saturation, except the measurements when S=1 in multiple-specimen method. This is possibly because of the potential bad contact between vertically inserted TR-1 sensor and highly saturated soil (S~1) in multiple-specimen method as previous discussed. Figure 2-7(b) shows similar observations, but has even larger error (Err~5%) above critical saturation.

Figure 2-8(a) shows a comparison of the error value between three methods for all 12 sands. The overall average error value is about 1.1%, 0.7%, and 0.9% for modified hanging column, staged-drying, and multi-specimen methods, respectively. When $S>S_{crit}$, the error value from modified hanging column method (Err~1.5%) is higher than that from staged-drying

(*Err*~0.6%) or multiple-specimen method (*Err*~0.8%), interpreted to correspond to the forced convection potentially occurring near the SH-1 sensor caused by water movement and free convection caused by larger heat pulse emitted by SH-1 sensor in modified hanging column method as previously discussed. Since the flow rate of water is a factor influencing forced convection, the unsaturated flow equation is employed as following to illustrate the observations (Lu and Likos, 2004):

$$q = -k(h_m)\left(\frac{dh_m}{dz} + 1\right) \quad (1)$$

where q is the flow rate, dh_m is the change of matric suction head, dz is the change of elevation head, and $k(h_m)$ is the unsaturated hydraulic conductivity dependent on the matric suction head. Furthermore, the unsaturated hydraulic conductivity ($k(h_m)$) could be indirectly related to D_{10} using the Gardner (1958) equation in the form:

$$k(h_m) = k_s exp(\beta h_m) \quad (2)$$

, and the Hazen (1892) Equation in the form:

$$k_s = C(D_{10})^2 \quad (3)$$

where k_s is the saturated hydraulic conductivity, β is the soil parameter that describe the reduction in hydraulic conductivity and water content, and C is the empirical coefficient.

Thus, as a physical property of soil, D_{10} is considered as a factor that may have an impact on the forced convection occurring near SH-1 sensor. Figure 2-8(b) shows that the error when $S<S_{crit}$ increases with the increasing D_{10} for 12 sands in modified hanging column method. This reflects that the error in modified hanging column method is possibly caused by forced convection related to the flow rate which may vary depending on the D_{10} of the sample.

Table 2-2 summarizes the approximate amount of time required to produce robust TRDCs using three methods for one sample. The total averaged time for modified hanging

column method is about 541 h (~23 days), which is the longest among all three methods. This time ranges from 384 h (~16 days) to 744 h (~31 days) among all 12 specimens. During the test of modified hanging column method, the specimens undergo two different periods: drainage and evaporation periods. The drainage period only takes about 4 days, while the evaporation period takes up to 27 days. Compared to the same type of test conducted by Likos *et al.* (2012), which was called automated Tempe cell test, the testing time of the modified hanging column method in this study is more than 4 times longer than the test from Likos *et al.* (2012). This large difference is likely due to the finer and less uniform soil types used in this study when compared to the samples from Likos *et al.* (2012). Additionally, the test environment may affect the testing time; for example, some samples were tested in the humid summer (room relative humidity near 50%), of which the evaporation process is much slower than the dry winter (room relative humidity near 20%).

Even though the staged-drying and the multiple-specimen methods could be used to obtain TRDCs in 10 days and in one day respectively, they produce relatively weaker TRDCs containing discrete points compared to the much more continuous TRDCs by modified hanging column method. Moreover, the critical saturation (S_{crit}) could be more easily obtained from this continuous TRDC by modified hanging column method. Figure 2-9 shows the results from variability tests for single location and multiple locations. The coefficients of variance are 0.013 and 0.016 for single location and multiple locations respectively, which indicates that the greater scatter may be expected in staged-drying and multiple-specimen tests with the TR-1 sensor inserted into different locations.

2.4 SUMMARY AND CONCLUSIONS

Three different laboratory methods, including modified hanging column, staged-drying, and multiple-specimen, were used to produce TRDCs for 12 sandy soils. The modified hanging column method using SH-1 sensor was found to overestimate ρ when $S>S_{crit}$ potentially due to the presence of forced convection likely caused by water movement near the SH-1 sensor and free convection caused by larger heat pulse created by the SH-1 sensor. Whereas the staged-drying and multiple-specimen methods using TR-1 sensor produce higher ρ than the modified hanging column method when $S<S_{crit}$ because of potential higher contact resistance between the soil particles and the TR-1 sensor. The errors associated with the SH-1 and TR-1 sensors were analyzed, and verify the above comparisons. The modified hanging column method requires the longest testing time, ranging from 16 days to 31 days dependent on the soil types and the testing environment. However, the modified hanging column method could produce much more continuous TRDCs showing well-defined regimes with S_{crit} compared to the staged-drying and multiple-specimen methods which require only 10 days and 1 day for one sample respectively. In addition, the staged-drying and multiple-specimen methods may have greater variability attributed to the sample inhomogeneity.

2.5 NOTATION

The following symbols are used in this chapter:

C = empirical coefficient in Hazen (1892) equation
C_c = coefficient of curvature
C_u = coefficient of uniformity
D_{10} = grain size at 10% finer by mass
D_{50} = median grain size by mass
dh_m = change of suction head
dz = change of elevation head
e = void ratio
e_{min} = minimum void ratio
e_{max} = minimum void ratio

G_s = specific gravity of soil solids
$k(h_m)$ = hydraulic conductivity dependent on suction head
k_s = saturated hydraulic conductivity
S = degree of saturation
S_{crit} = saturation at sharp transition in TRDC
β = soil parameter that describe the reduction in hydraulic conductivity and water content in Gardner (1958) equation
λ = thermal conductivity

2.6 REFERENCES

ASTM D 2487. (2011). "Standard Practice for Classification of Soils for Engineering Purposes (Unified Soil Classification System)."

ASTM D 4318-10. (2010). "Standard Test Methods for Liquid Limit, Plastic Limit, and Plasticity Index of Soils."

ASTM D 854-10. (2010). "Standard Test Methods for Specific Gravity of Soil Solids by Water Pycnometer."

ASTM D 6836-02. (2008). "Standard Test Methods for Determination of the Soil Water Characteristic Curve for Desorption Using Hanging Column, Pressure Extractor, Chilled Mirror Hydrometer, or Centrifuge."

ASTM D 422-63. (2007). "Standard Test Method for Particle-Size Analysis of Soils."

Bareither, C. A., Edil, T. B., Benson, C. H., and Mickelson, D. M. (2008). "Geological and Physical Factors Affecting the Friction Angle of Compacted Sands." *Journal of geotechnical and geoenvironmental engineering*, *134*(10), 1476-1489.

Brandon, T.L., Mitchell, J.K., and Cameron, J.T. (1989). "Thermal Instability in Buried Cable Backfills." *J. of Geotechnical Engineering*, ASCE, 115(1), 38-55.

Campbell, G. S. (2011), "Producing Thermal Dryout Curves for Buried Cable Applications." Application Note 13994-01 AN, Decagon Devices, Inc., Pullman WA.

Campbell, G.S., Jungbauer, J.D., Bidlake, W.R., and Hungerford, R.D. (1994). "Predicting the Effect of Temperature on Soil Thermal Conductivity." *Soil Science*, 158(5), 307-313.

Campbell, G. S. (1985). *Soil Physics with BASIC: Transport Models for Soil-plant Systems* (Vol. 14). Elsevier Science

Côté, J., and Konrad, J. M. (2005). "A Generalized Thermal Conductivity Model for Soils and Construction Materials." *Canadian Geotechnical Journal, 42*(2), 443-458.

Dayan, A., Merbaum, A. H., and Segal, I. (1984). "Temperature Distributions around Buried Pipe Networks in Soil with a Temperature Dependent Thermal Conductivity." *International journal of heat and mass transfer*, *27*(3), 409-417.

Decagon Devices. (2014) "KD2 Pro Thermal Properties Analyzer" Operator's Manual. Decagon Devices, Inc., Pullman WA.

Donazzi, F., Occhini, E., and Seppi, A. (1979). "Soil Thermal and Hydrological Characteristics in Designing Underground Cables." In *Proceedings of the Institution of Electrical Engineers* (Vol. 126, No. 6, pp. 506-516). IET Digital Library.

Fan, R., Jiang, Y., Yao, Y., Shiming, D., and Ma, Z. (2007). "A Study on the Performance of a Geothermal Heat Exchanger under Coupled Heat Conduction and Groundwater Advection." *Energy*, *32*(11), 2199-2209.

Farouki, O. T. (1981). *Thermal Properties of Soils* (No. CRREL-MONO-81-1). COLD REGIONS RESEARCH AND ENGINEERING LAB HANOVER NH.

Freitas, D. S., Prata, A. T., and de Lima, A. J. (1996). "Thermal Performance of Underground Power Cables with Constant and Cyclic Currents in Presence of Moisture Migration in the Surrounding Soil." *Power Delivery, IEEE Transactions on, 11*(3), 1159-1170.

Gouda, O. E., El Dein, A. Z., and Amer, G. M. (2011). "Effect of the Formation of the Dry Zone around Underground Power Cables on their Ratings." *Power Delivery, IEEE Transactions on*, *26*(2), 972-978.

Guymon, G. L., Berg, R. L., and Hromadka, T. V. (1993). *Mathematical Model of Frost Heave and Thaw Settlement in Pavements* (No. CREEL-93-2). COLD REGIONS RESEARCH AND ENGINEERING LAB HANOVER NH.

Kersten, M. S. (1949). *LABORATORY RESEARCH FOR THE DETERMINATION OF THE THERMAL PROPERTIES OF SOILS.* MINNESOTA UNIV MINNEAPOLIS ENGINEERING EXPERIMENT STATION.

Kluitenberg, G. J., J. M. Ham, and K. L. Bristow, (1993). Error Analysis of the Heat Pulse Method for Measuring Soil Volumetric Heat Capacity Soil Sci. Soc. Am. J. 57:1444-1451

Likos, W. (2013). "Modeling Thermal Conductivity Dryout Curves from Soil-Water Characteristic Curves." *J. Geotech. Geoenviron. Eng.*, 10.1061/(ASCE)GT.1943-5606.0001078 , 04013056.

Likos, W. J., Olson, H. S., and Jaafar, R. (2012). "Comparison of Laboratory Methods for Measuring Thermal Conductivity of Unsaturated Soils." *GeoCongress 2012*

Li, Y., Wu, C., Xing, X., Dou, D., and Yu, Y. (2013). Testing Backfill's Thermal Conductivity Improves Operations. *Oil & gas journal*, *111*(10), 110-116.

Lu, N. and Likos, W. J. (2004). *Unsaturated Soil Mechanics*. J. Wiley.

Sakaki, T., Limsuwat, A., Smits, K. M., and Illangasekare, T. H. (2008). "Empirical Two-Point A-Mixing Model for Calibrating the ECH2O EC-5 Soil Moisture Sensor in Sands." *Water Resources Research*, *44*(4).

Shelton, J. (1975). Underground Storage of Heat in Solar Heating Systems. *Solar Energy*, *17*(2), 137-143.

Smits, K. M., Sakaki, T., Limsuwat, A., and Illangasekare, T. H. (2010). "Thermal Conductivity of Sands under Varying Moisture and Porosity in Drainage - Wetting Cycles." *Vadose Zone Journal*, *9*(1), 1-9.

Smits KM, Sakaki T, Limsuwat A, and Illangasekare TH (2009) Determination of the Thermal Conductivity of Sands under Varying Moisture, Drainage/Wetting, and Porosity Conditions: Applications in Near-Surface Moisture Distribution Analysis. In: Proceedings of AGU Hydrology Days 2009

Southen, J. M., and Rowe, R. K. (2005). Modelling of Thermally Induced Desiccation of Geosynthetic Clay Liners. *Geotextiles and Geomembranes*, *23*(5), 425-442.

Woodward, N. R. and Tinjum, J. M. (2012). "Impact of Moisture Migration on Thermal Resistivity Testing in Unsaturated Soil." *GeoCongress 2012*

2.7 TABLES

Table 2-1. Summary of properties for twelve sands

Sample	USCS	D_{50} (mm)	D_{10} (mm)	C_u	C_c	Fines (%)	G_s	e_{min}	e_{max}
SP1	SP	0.38	0.18	2.4	1.0	0.6	2.65	0.49	0.82
SP2	SP	0.29	0.18	1.8	0.9	1.8	2.68	0.55	0.73
SP3	SP	0.34	0.12	3.4	1.6	4.8	2.68	0.46	0.77
SP5	SP	0.22	0.15	1.6	1.0	1.1	2.66	0.51	0.75
SP6	SP	0.77	0.24	5.0	0.6	3.1	2.67	0.33	0.56
SP7	SP	0.50	0.26	2.2	1.0	1.8	2.65	0.43	0.66
SP-SM8	SP-SM	0.19	0.08	2.6	1.3	7.4	2.70	0.47	0.72
SW1	SW	0.62	0.13	7.5	1.0	3.1	2.66	0.31	0.64
SW-SM2	SW-SM	0.46	0.08	8.7	1.4	9.1	2.68	0.34	0.64
SW-SM3	SW-SM	0.51	0.10	7.0	1.0	7.8	2.72	0.35	0.59
SM1	SM	0.11	0.05	2.6	1.1	20.8	2.68	0.51	0.86
SM2	SM	0.13	0.05	3.2	1.0	19.9	2.75	0.55	0.81

Table 2-2. Comparison of approximate time to obtain TRDCs

Test Method	Modified Hanging Column (h)	Staged-drying (h)	Multiple-specimen (h)
Preparation time	2	2	2
Testing time	539	240	2
Total time	541	242	4

2.8 FIGURES

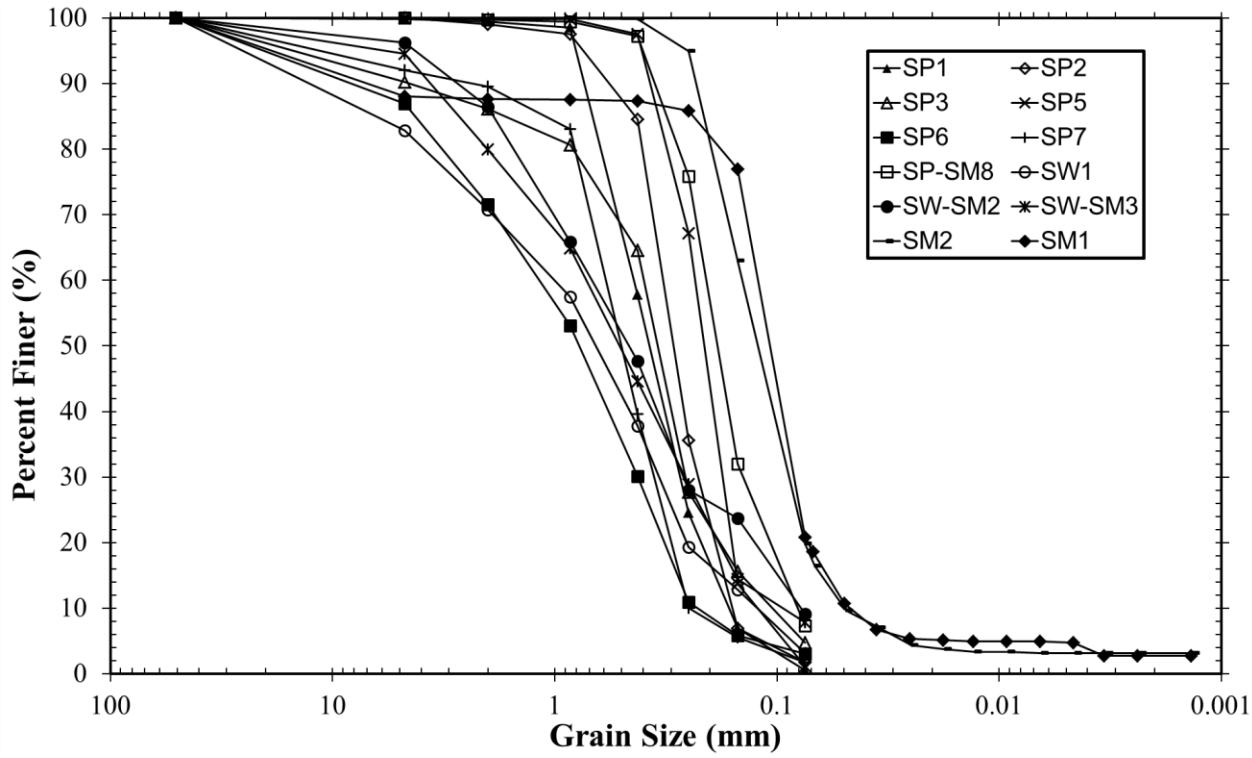

Figure 2-1. Grain-size distribution curves for twelve sands

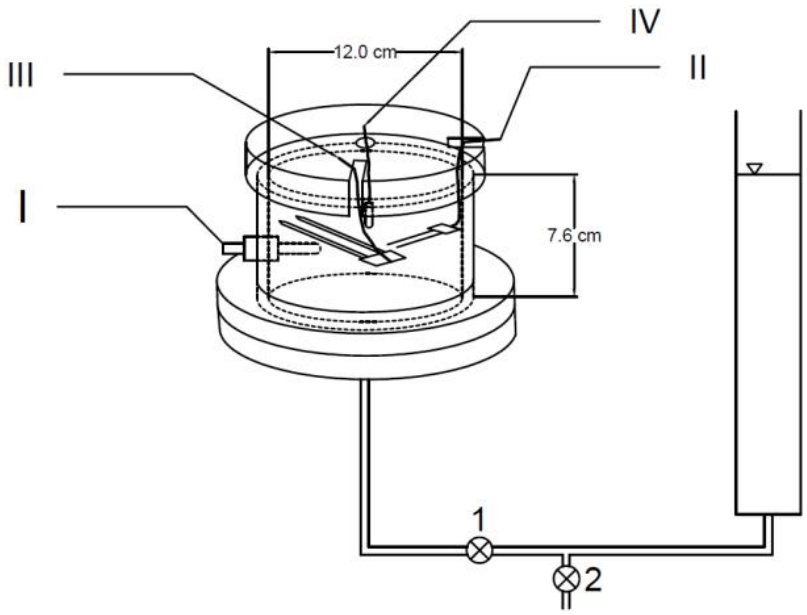

Figure 2-2. Schematic of modified hanging column apparatus

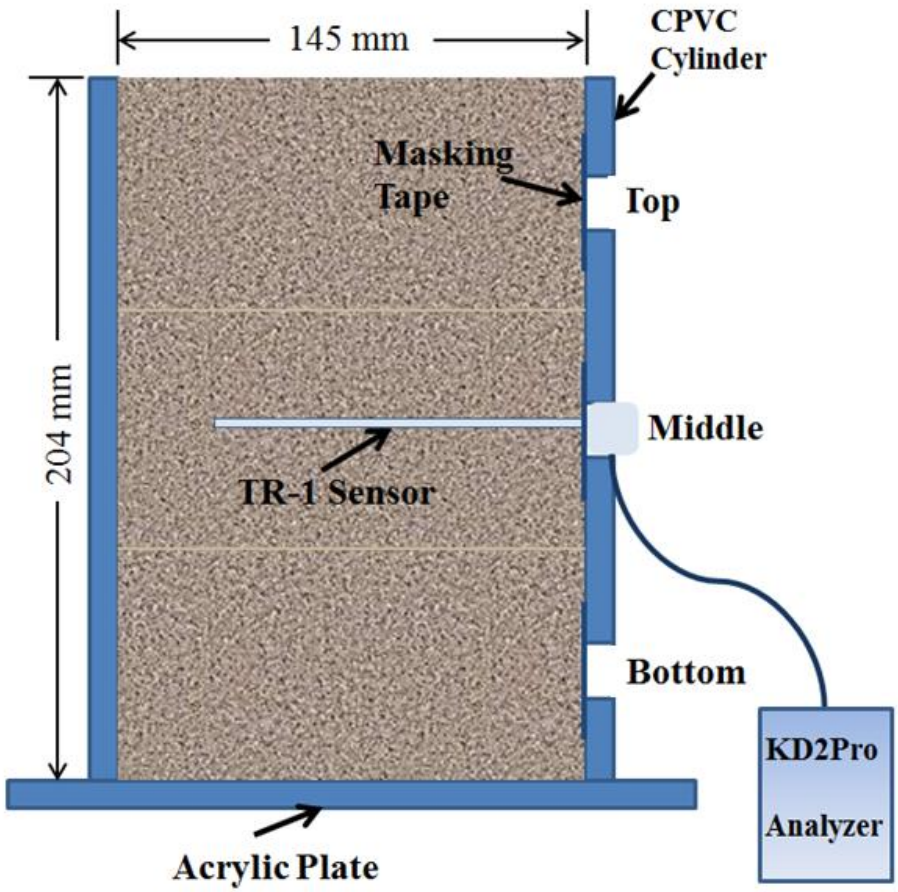

Figure 2-3. Schematic of staged-drying test apparatus

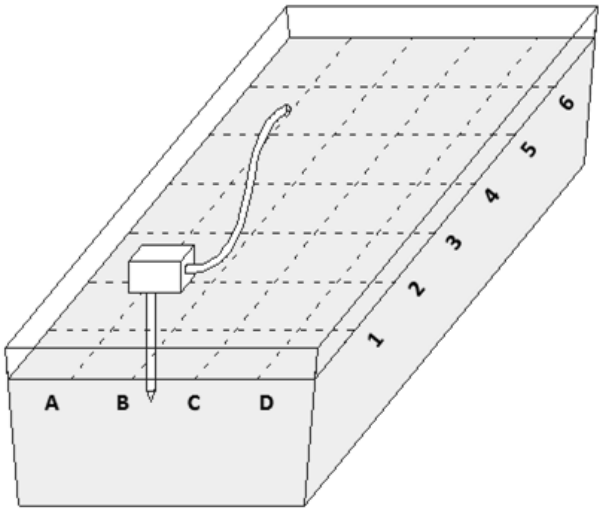

Figure 2-4. Apparatus of variability test for multiple location measurements (Likos et al., 2012)

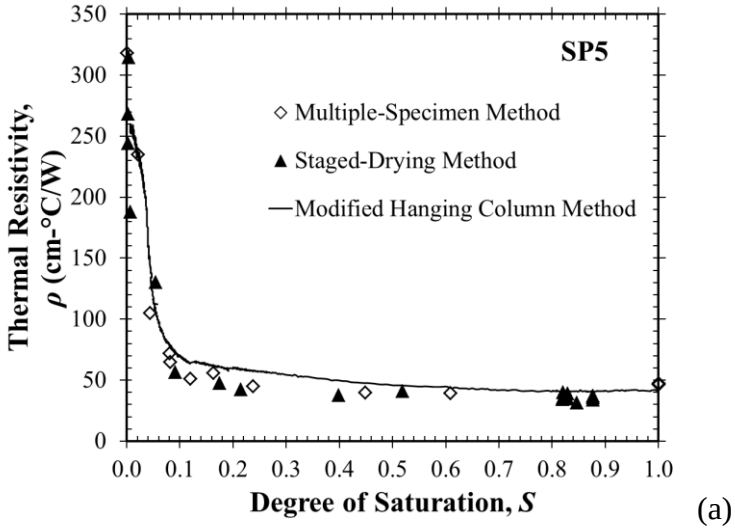

(a)

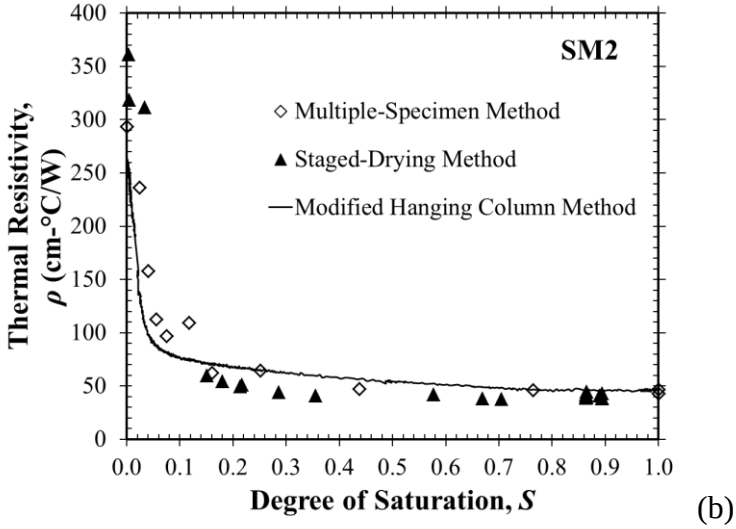

(b)

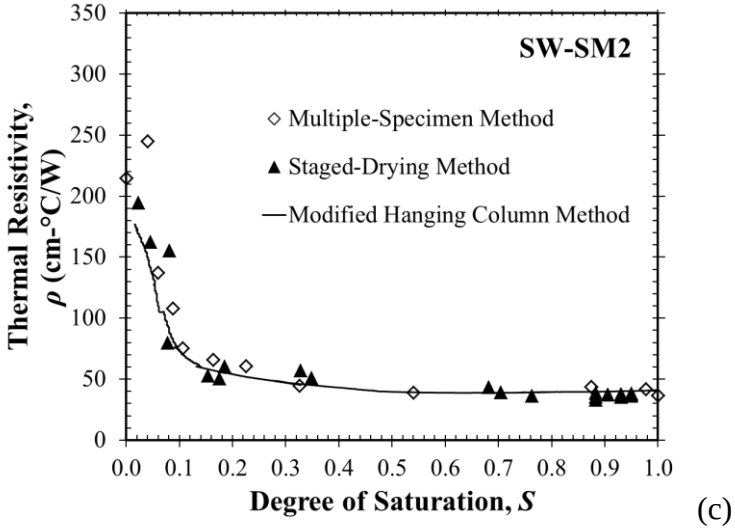

(c)

Figure 2-5. TRDCs obtained using three testing methods for (a) SP5, (b) SM2, and (c) SW-SM2

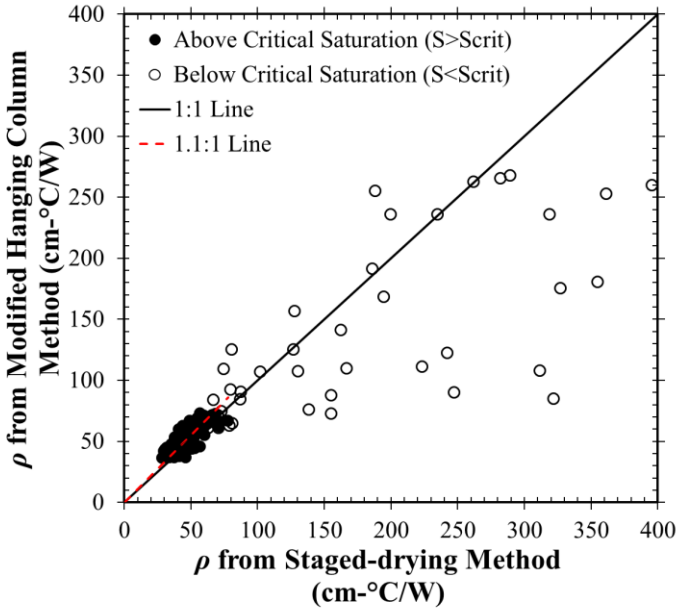

(a)

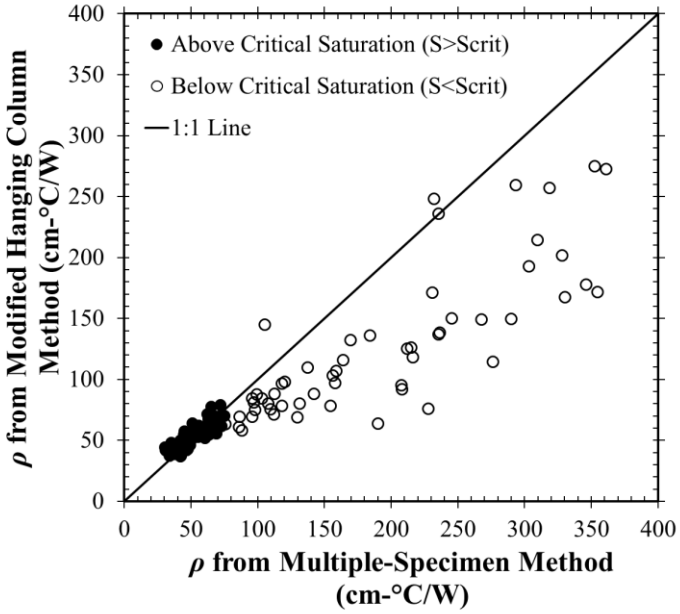

(b)

Figure 2-6. Comparison of ρ values (a) between modified hanging column and staged-drying methods; (b) between modified hanging column and multiple-specimen methods for all 12 sands

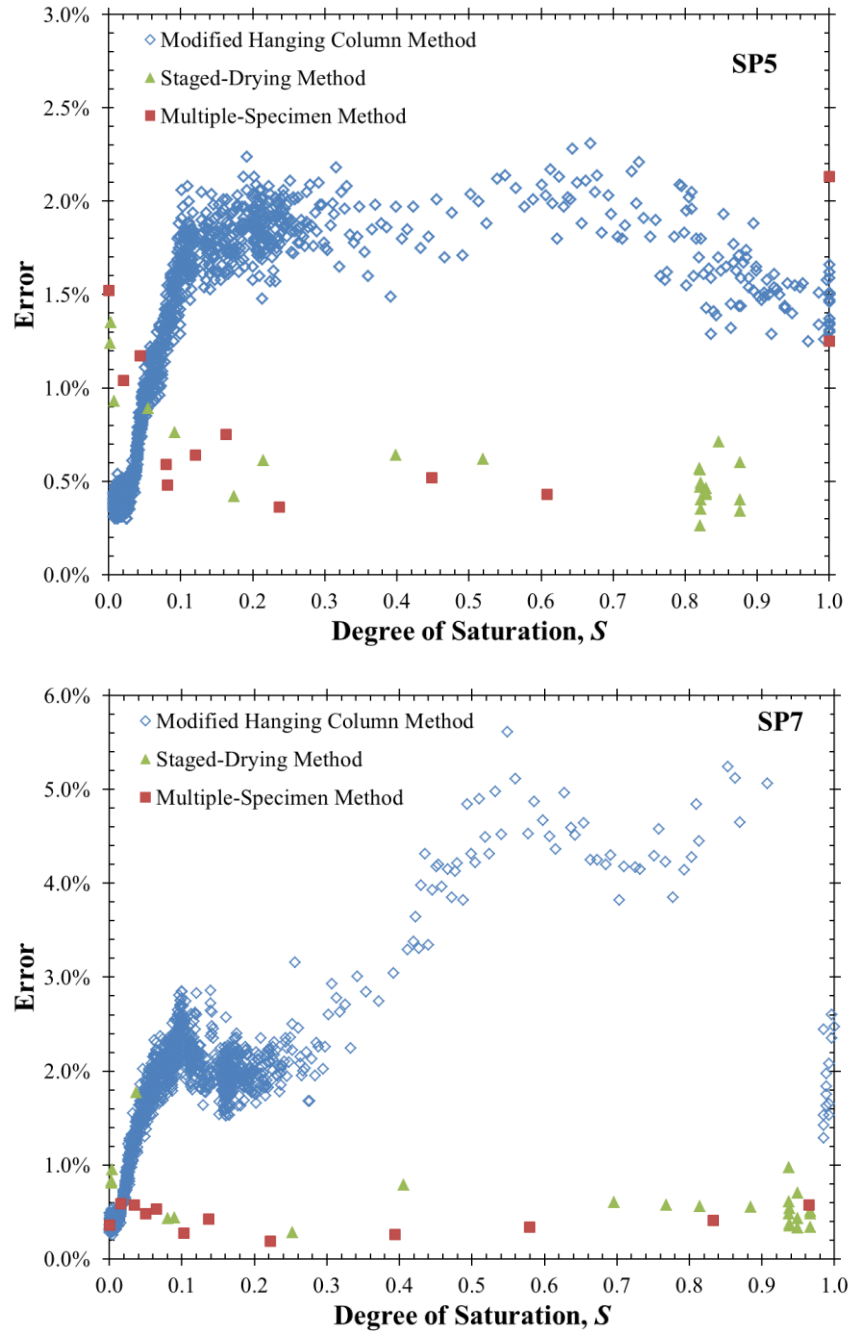

Figure 2-7. The relationship between errors and degree of saturation in three methods for (a) SP5; and (b) SP7

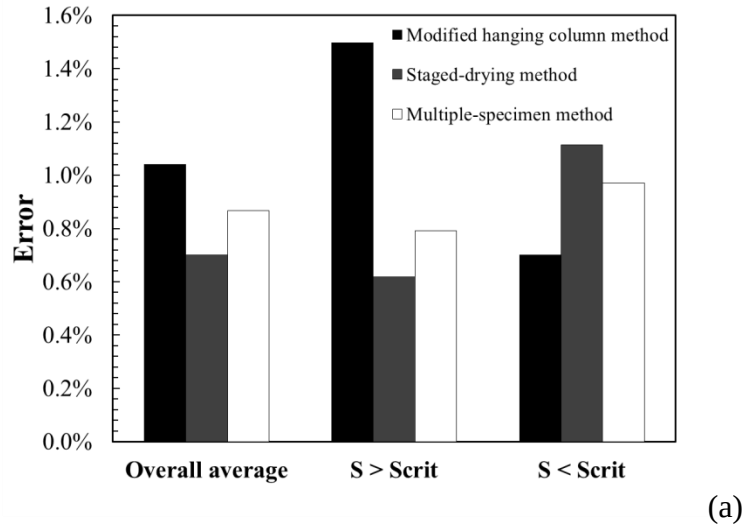

(a)

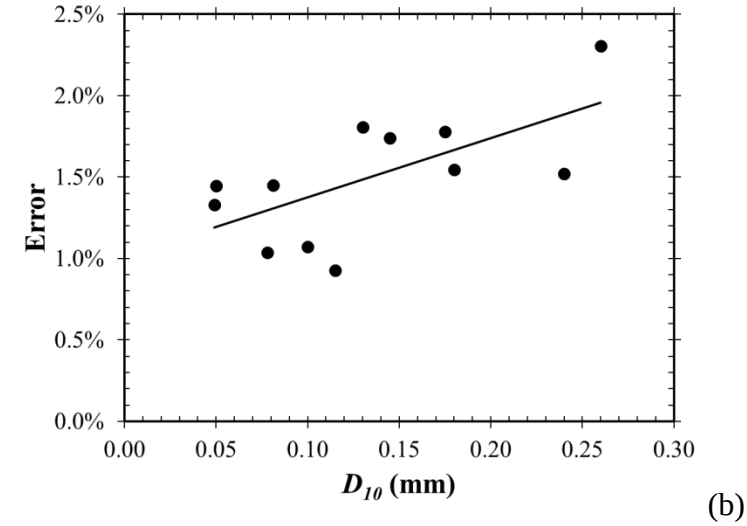

(b)

Figure 2-8. (a) Comparison of error values between three methods; (b) relationship between error and D_{10}

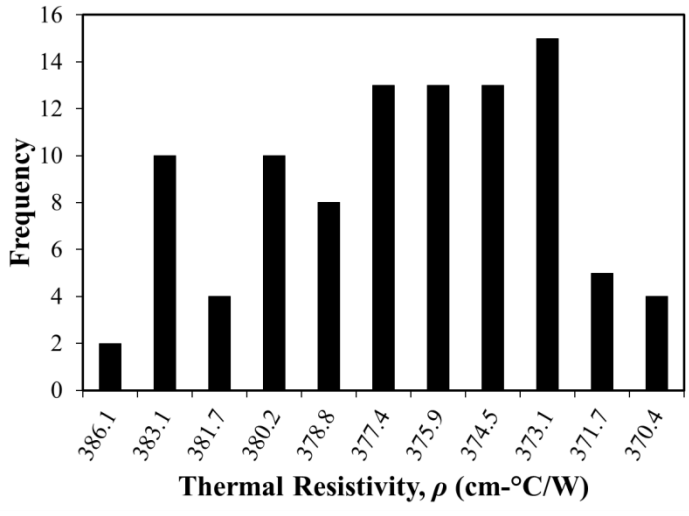

(a)

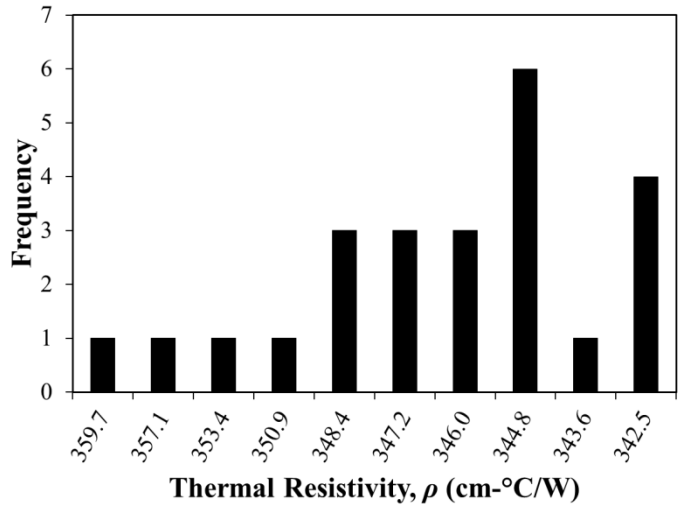

(b)

Figure 2-9. Results from variability test for (a) SH-1 single location measurements; and (b) TR-1 multiple locations measurements

CHAPTER THREE

TWO NEW MATHEMATICAL MODELS FOR THERMAL CONDUCTIVITY DRY-OUT CURVES OF COARSE-GRAINED SOILS

3.1 INTRODUCTION

In recent decades, thermal-related studies have become increasingly relevant in geotechnical engineering. As a result, the knowledge of thermal properties of porous media is gaining popularity for many engineering applications. Examples of historical and recent applications include underground storage systems, backfill for buried power cables, estimation of frost heave and thaw settlement in cold regions, energy foundations, and ground-source heat exchangers (Shelton, 1975; Brandon *et al*., 1989; Guymon *et al*., 1993; Brandl, 2006; Fan *et al*., 2007).

The three mechanisms of heat transfer through soils are conduction, convection, and radiation. Of these three mechanisms, convection and radiation are often considered negligible for soils compared to conduction (Farouki, 1981). Thus, the thermal conductivity (λ) that characterizes the rate of heat transfer through the soil is the predominant factor for soil thermal properties. In addition, since latent heat transfer can have a significant effect due to water evaporation and condensation, the thermal conductivity described herein is actually the apparent thermal conductivity, and includes the sum effect of conduction through particles, water, and air and the latent heat transfer from water evaporation and condensation (Farouki, 1981; Campbell *et al*., 1994).

In near ground surface applications, soil is often unsaturated and thus includes multiple phases (i.e., solid, liquid and gas). A common value λ of soil solid varies from 1.0 to 9.0 W/mK,

whereas λ values for water and air are 0.6 and 0.024 W/m·K, respectively (Johansen, 1975; Côté and Konrad, 2005). Because heat flows through these three phases with different conductivities, the bulk or effective thermal conductivity of porous media is significantly dependent on the degree of pore water saturation. Furthermore, thermal conductivity of soil also depends on soil mineralogy, bulk density and temperature. The dependency of these factors has been investigated in many previous studies (Johansen, 1975; Farouki, 1981; Hopmans and Dane, 1986; Brandon and Mitchell, 1989; Campbell *et al*., 1994; Côté and Konrad, 2009; Smits *et al.*, 2010).

The purpose of this paper is to model the relationship between thermal conductivity and degree of pore water saturation for coarse grained soils at room temperature. Two new mathematical models are proposed based upon observations from two similar previous studies (Smits *et al.*, 2010; Likos *et al.*, 2012) and test results obtained in this study. Empirical relationships between the model parameters and soil physical parameters are also investigated to examine the efficacy of predicting λ from more easily measured soil physical parameters. Performance of the proposed models is compared to a variety of models available in the literature (e.g., Johansen, 1975; Campbell, 1985; Hu *et al.* 2001; Côté and Konrad, 2005; Lu *et al.*, 2007; Likos, 2013).

3.2 BACKGROUND

3.2.1 Thermal Conductivity Dry-out Curves

Thermal conductivity dry-out curves (TCDCs) quantify the non-linear relationship between effective thermal conductivity (λ) and degree of pore water saturation (S). Figure 3-1 is an idealized TCDC typical of coarse-grained soils at room temperature. The curve is divided into 4 distinct regimes based on several observations from previous studies (Campbell, *et al.*, 1994;

Smits *et al.*, 2010; Likos *et al.*, 2012; Likos, 2013). In regime I, while *S* decreases from 1 to a lower limit (S_b), λ remains relatively constant at a maximum value corresponding to saturation (λ_{sat}). The air, existing as small occluded bubbles in the pores, has a minimal effect on the heat transfer; thus, the heat largely migrates through saturated grain-water-grain pathways (Smits *et al.*, 2009). Within the regime II, λ decreases slowly in a generally linear trend as *S* decreases. As the water phase in the large pores is displaced by air, heat transfer is forced to occur through longer and fewer grain-water-grain pathways. When *S* drops below some critical saturation (S_c) into the regime III, λ starts to decrease dramatically because the water phase is no longer continuous and forms isolated liquid bridges between soil grains. Therefore, the heat transports less effectively through this weaker and more tortuous grain-water-grain pathway. Additionally, the reduction of water vapor recirculation could lead to the loss of latent heat transport, causing the apparent thermal conductivity to decrease (Campbell *et al.*, 1994). In the final regime (regime IV), λ is essentially at a constant value (λ_{dry}) between $S = 0$ and $S = S_d$. The potential reason for this observation is that the weak water liquid bridges break up, and the water forms thin films absorbed on the finer particles. The heat in this regime can only transfer through the poor grain-to-grain contact, thus leveling λ to a minimum value.

3.2.2 Previous TCDC Models

A number of models have been proposed for modeling the relationship between λ and *S*. Of these models, most have been developed based on the normalized thermal conductivity theory first described by Johansen (1975). Normalized thermal conductivity, or Kersten's number (K_e) is in the form:

$$K_e = \frac{\lambda - \lambda_{dry}}{\lambda_{sat} - \lambda_{dry}} \quad (4)$$

where λ is normalized between 0 and 1. When the soil is completely dry ($\lambda = \lambda_{dry}$), K_e is 0. When the soil is fully saturated ($\lambda = \lambda_{sat}$), K_e is 1. This Kersten's number is also a function of saturation (i.e. $K_e = f(S)$). Based on experiment results obtained from Kersten (1949), Johansen (1975) proposed the first empirical relationship between K_e and S for unfrozen coarse grained soils:

$$K_e = f(S) = 0.7 \log(S) + 1 \qquad (S > 0.05) \tag{5}$$

Hu *et al.* (2001) established an empirical relationship for K_e based on the relationship between capillary pressure and saturation. This approach utilized the finite element method to calculate a steady-state temperature field by applying heat through unsaturated porous media. An equation for the K_e-S relationship was proposed in the form:

$$K_e = f(S) = 0.1811 \ln(S) + 0.9878 \tag{6}$$

Côté and Konrad (2005) proposed a model for correlating K_e with S based on empirical observation from over 650 test results for unfrozen and frozen moist soils. That model is defined as:

$$K_e = f(S) = \frac{\kappa S}{1+(\kappa-1)S} \tag{7}$$

where κ is an empirical parameter dependent on soils type in the unfrozen or frozen state. A κ value of 3.55 was suggested for fine and medium sand similar to the soil type used in the current study.

Based on heat-pulse measurements conducted on twelve soils, Lu *et al.* (2007) developed another form of model to present K_e as:

$$K_e = f(S) = exp\{\alpha[1 - S^{(\alpha-1.33)}]\} \tag{8}$$

where α is an empirical parameter dependent on soil type. For coarse-grained soils, α was suggested to be 0.96.

Campbell (1985, 2011) employed the weighted sum theory from de Vries (1963) to propose a model for predicting λ in the form:

$$\lambda = \lambda_{sat} g + \lambda_{dry}(1 - g) + 2.8n(\theta - \theta_{sat} g) \tag{9}$$

$$g = \frac{1}{1+(\frac{\theta}{\theta_o})^{-5}} \tag{10}$$

where θ is the volumetric water content, θ_{sat} is the saturated volumetric water content, n is the porosity, g is an empirical weighing factor, and θ_o is a cutoff volumetric water content for liquid return flow in soil, and can be estimated from the clay fraction (m_c) using the following equation:

$$\theta_o = 0.3073 m_c + 0.0334 \tag{11}$$

Likos (2013) proposed a new approach to model TCDCs through the measurements of the soil-water characteristic curve (SWCC). This model adapted the bimodal formulation of the Brooks and Corey (1964) (BC) SWCC function to link the thermal conductivity (λ) to the matric suction (ψ) using the following equation:

$$\lambda = \begin{cases} \lambda_{dry} + \left(\lambda_{crit} - \lambda_{dry}\right)\left(\frac{\psi_{crit}}{\psi}\right)^{\beta'}; & \psi_{crit} < \psi \\ \lambda_{crit} + (\lambda_{sat} - \lambda_{crit})\left(\frac{\psi_b}{\psi}\right)^{\beta}; & \psi_b < \psi < \psi_{crit} \\ \lambda_{sat}; & \psi < \psi_b \end{cases} \tag{12}$$

where λ_{crit} is the critical thermal conductivity where λ starts to drop abruptly, ψ_{crit} is the critical suction corresponding to λ_{crit}, ψ_b and β are the fitting parameters for the low-suction portion ($\psi<\psi_{crit}$) of the curve, and β' is a fitting parameter for the high-suction portion ($\psi_{crit}<\psi$) of the curve. The parameters ψ_b and β can be found by best fitting a unimodal BC function on a measured SWCC. Based on limited experiments conducted for seven sandy soils, the empirical relationships, $\beta' = 2.8\beta$ and $\lambda_{crit} = 0.58\lambda_{sat}$ were suggested for predicting the TCDC.

3.3 PROPOSED TCDC MODELS

Since most previous TCDC models have been derived based on the discrete λ measurements, those models are unlikely to effectively capture the four different regimes of the TCDC. Even though the model from Likos (2013) was constructed based on much more continuous λ measurements, the initial flat regime (regime I) was not successfully captured by the model. Therefore, based upon the observations from previous study (i.e. Smits *et al*., 2010 and Likos *et al.*, 2012) and the current study, two new piecewise models were proposed for the TCDC. The first proposed model (denoted Model I) consists of four linear segments defined by the following equation:

$$\lambda = \begin{cases} \lambda_{dry}; & S \leq S_d \\ \gamma(S - S_c) + \lambda_c; & S_d \leq S \leq S_c \\ \beta(S - S_c) + \lambda_c; & S_c \leq S \leq S_b \\ \lambda_{sat}; & S_b \leq S \end{cases} \tag{13}$$

where S_d is the degree of saturation where regime III transitions into regime IV, S_c is the critical degree of saturation where λ starts to drop abruptly, λ_c is the critical thermal conductivity corresponding to S_c, and S_b is the degree of saturation where regime I transitions into regime II. The parameters β and γ capture the decreasing rates of thermal conductivity in regime II and regime III, respectively.

The second proposed model (denoted Model II) is composed of three segments in the form:

$$\lambda = \begin{cases} \lambda_{dry}; & S \leq S_d \\ \lambda_{sat}\sqrt[n]{\frac{S - S_d}{S_b - S_d}}; & S_d < S \leq S_b \\ \lambda_{sat}; & S_b \leq S \end{cases} \tag{14}$$

where *n* is a parameter that characterizes the decreasing rate of thermal conductivity in regime II and regime III. This model uses a non-linear function instead of two separate linear functions in Model I to describe the regime II and regime III.

3.4 MATERIALS AND METHODS

3.4.1 Test materials

Nine natural sandy soils were selected to determine experimental TCDCs and evaluate model performance. These soils included: (*i*) eight sandy soils from the University of Wisconsin-Madison Soil Bank, which contains total 30 sands collected from various geological deposits in Wisconsin (Bareither *et al*., 2008), and (ii) a sandy soil from Grand Marsh, Wisconsin. Figure 3-2 shows grain-size distribution (GSD) curves for the nine sandy soils obtained using mechanical sieve analysis (ASTM D422). Additional hydrometer tests were performed on two soils (SM1 and SM2) to successfully capture D_{10} from the GSD curves. For those soils with more than 5% fines, the portion passing the No.40 sieves was sampled for plastic limit and liquid limit tests (ASTM D4318).

According to the Unified Soil Classification System (USCS) based on ASTM D2487, results from mechanical sieve analysis, hydrometer tests, plastic limit and liquid limit tests were used to classify the materials into 3 soil types: (*i*) Poorly Graded Sand, SP; (*ii*) Silty Sand, SM; and (*iii*) Poorly Graded Sand with Silt, SP-SM. Table 3-1 summarizes material properties including D_{50}, D_{10}, coefficient of uniformity (C_u), coefficient of curvature (C_c), fines content, specific gravity of the solids (G_s). D_{50}, D_{10}, C_u and C_c and fines content were determined from GSDs. The specific gravity was determined using ASTM D854.

3.4.2 Modified Hanging Column Test Procedures

Soil-water characteristic curves (SWCCs) and TRDCs were obtained concurrently along an initial drying path (*i.e.*, drainage from $S = 1$) using an instrumented hanging column apparatus (Smits *et al.*, 2010; Likos *et al.*, 2012). The apparatus (Figure 3-3) consists of an acrylic confining sleeve, a perforated bottom plate, and a top cap. The bottom plate includes a brass screen designed to support a high-air-entry nylon membrane (diameter = 142 mm, pore size = 0.2 μm, air-entry pressure = 340 kPa), through which suction is applied to the sand via a hanging-column water system (ASTM D6836-02).

Sensors were directly buried in the sand to obtain measurements of suction, moisture content, temperature, and thermal resistivity/conductivity as suction was increased or decreased using the hanging water column. Measurements were interpreted to produce a continuous SWCC and TRDC along either a continuous drying or wetting path. The sensor for measuring matric suction (denoted I in Figure 3-3) is a small-tip tensiometer inserted through a plastic fitting on the side wall of the cell, embedded into the soil, and connected to a differential pressure transducer (Model P55D, Validyne Engineering Corp., Northridge, CA) and data-logger system. The thermal sensor (II) is a dual-needle transient thermal probe (SH-1) connected to a KD2Pro data-acquisition system (Decagon Devices, Pullman, WA) for measuring soil thermal properties. The moisture sensor (III) is a dual-prong dielectric moisture sensor (ECH_2O EC-5, Decagon Devices, Pullman, WA) connected to an Decagon Em50 data logger. Raw data acquired from the moisture sensor was independently calibrated for each test material using the two-point α-mixing model from Sakaki *et al*. (2008). The temperature sensor (IV) was embedded into the top portion of the soil and connected to the Em50 data logger.

For the tests reported herein, sands were compacted to an initial void ratio (*e*) of 0.6. Dry sand, which was dried in an oven at 105 °C for 24 h, was compacted directly into the confining sleeve in four equal layers to a height of about 1 cm below the top edge of the cell. This resulted in a typical specimen height of 6.6 cm. The tensiometer, moisture sensor, and SH-1 sensor were embedded in the sand between the 2nd and the 3rd layers. Sakaki *et al.* (2008) conducted experiments to show that the bulk sampling volume of the EC-5 moisture sensor is approximately 18 cm^3, comprising 2 cm (parallel to prongs) × 1 cm (perpendicular to prongs) × 9 cm (longitudinal including sensor head). Thus, for a horizontally oriented moisture sensor, the water content measurement represents some average of the material 1 cm above and below the sensor. Thus the water content measurement obtained in the present apparatus is representative of a vertical region of sand equal to about 30% of the overall specimen height. The temperature sensor was inserted through a vent in the top cap and buried in the top portion of the sand after compaction.

After packing, valve 1 (Figure 3-3) was opened to wet the membrane and the specimen from bottom to top until approximately 1 cm water ponded on the top of the sand surface. The water level in the cell and standpipe was then brought down to the midpoint of the cell at the elevation where the tensiometer, moisture sensor, and thermal probe were located. Valve 2 was then partially opened to produce a slow drip from the water column at a rate of 6 to 10 s/drip, thereby slowly and continuously increasing the suction head applied to the sand. After the water in the standpipe was completely drained at a suction head of ~126.5 cm H_2O, the top cap of the confining sleeve was removed, and a small mechanical fan was set up near the top of the specimen for continued drying through evaporation. Matric suction, volumetric water content,

and thermal resistivity were continuously monitored until the volumetric water content of the sand reached a value less than about 0.01.

3.5 RESULTS AND DISCUSSION

3.5.1 Measured Thermal Conductivity Dry-out Curves and Model Demonstration

Figure 3-4 demonstrates the measured TCDC and SWCC for SP5, which is poorly graded sand. The four different regimes conceptualized previously in Section 3.2.1 are evident in this TCDC. The initial flat regime stops when $S = S_b \approx 0.78$. For all nine sands, the value of S_b was found to range from 0.6 to 0.9, approximately. After this flat regime, the thermal conductivity decreases slowly in a generally linear trend (regime II). The critical saturation, S_c, where regime II transitions into regime III, is approximately 0.1 for SP5. For all nine sands, the value of S_c was observed to be slightly lower than the residual saturation ($S_r \sim 0.15$) derived from the SWCC. The residual saturation (S_r) was obtained graphically by drawing tangent lines through the upper and lower portions on SWCC as shown in Figure 3-4. A potential reason for this observation is that the water phase is still continuous and formed as connected liquid bridges when S reaches S_r; thus, the heat could still transfer effectively through connected liquid bridges. Finnally, the thermal conductivity starts to decrease abruptly after S_c where the isolated liquid bridges form. At about $S = 0.025$, thermal conductivity tends to level off to a constant λ_{dry} (~0.4 W/m·K).

The TCDCs for nine sands were fit with two proposed models. Of these two proposed models, Model I includes eight fitting parameters (λ_{dry}, λ_{sat}, λ_c, γ, β, S_b, S_c, S_d), while Model II includes five fitting parameters (λ_{dry}, λ_{sat}, λ_c, n, S_b, S_d). These fitting parameters were optimized by implementing the models into a spreadsheet and using a multivariable solver to best match the measured TCDC and modeled TCDC. For Model I, two boundary constraints were applied in the form:

$$Boundary\ Constraints = \begin{cases} \lambda_{dry} = \gamma(S - S_c) + \lambda_c;\ when\ S = S_d \\ \lambda_{sat} = \beta(S - S_c) + \lambda_c;\ when\ S = S_b \end{cases} \quad (15)$$

The purpose of applying these two constraints is to make the Model I continuous at $S = S_b$ and $S = S_d$. The measured TCDC best fitted with Model I and Model II are shown in Figure 3-5(a) and Figure 3-5(b), respectively. In addition, the SWCC for each soil was best fitted with van Genuchten (1980) (VG) model in the form:

$$\frac{S - S_r}{1 - S_r} = \left[\frac{1}{1 + (\alpha\psi)^n}\right]^{1 - \frac{1}{n}} \quad (16)$$

where n, S_r and α are VG fitting parameters optimized to best match the measured SWCC and modeled SWCC. Table 3-2 summarizes the best-fitting parameters for Model I, Model II and van Genuchten model. The mean (μ) and standard deviation (σ) are also provided in Table 3-2.

3.5.2 Model Performance with Predicted Parameters

The best-fitting parameters for Model I and II were evaluated to find potential correlations with physical parameters (e.g., D_{50}, D_{10}, C_u, fines content) and the VG model parameters that characterize the SWCC. An acceptable correlation coefficient (R) was considered as ±0.6 in this study. Figure 3-6 and 3-7 show several key correlations for the fitting parameters in Model I and II. For Model I, S_c shows approximately 45% lower than the S_r obtained from VG model. The ratio between γ and β (γ/β) shows an inverse correlation with D_{50} and C_u. For Model II, an inverse correlation is evident between S_b and D_{50}. This D_{50} ranges from 0.1 to 0.5 mm in this study. The n parameters that characterizes regime II and III increase with decreasing D_{50} and C_u. To predict the TDDC using Model I and II, the following procedure is adopted:

1. For both Model I and II, optimized λ_{sat} and λ_{dry} are similar to the measured λ_{sat} and λ_{dry} in TCDC. Thus, the averaged λ_{sat} and λ_{dry} between Model I and II are used for predicted λ_{sat} and λ_{dry} in both models.
2. For Model I, the correlation between S_c and S_r from VG model (i.e., $S_c = 0.55S_r+0.06$) is employed for predicting S_c. In addition, the mean value of S_c is evaluated for predicting S_c (Fig. 3-8(a)). And the corresponding λ_c is determined as a fraction of λ_{sat}. From the optimized parameters, the averaged λ_c/λ_{sat} ratio is 0.65, with a standard deviation of 0.05. This ratio is in general accordance with the ratio (i.e. 0.58) reported for similar sandy soils by Likos (2013).
3. For Model I, predicted S_b and S_d are calculated using two boundary constraints in equation 12. For Model II, S_b is predicted using the correlation with D_{50} (i.e. $S_b = -0.807D_{50}+1$). This prediction is suitable for $D_{50} \leq 0.5$ mm. For the sand with $D_{50} > 0.5$ mm, a value 0.5 of S_b is suggested according to the TCDC results from Smits *et al.* (2010). As shown in Fig. 3-9(a), mean optimized S_d is approximately 0.024, and used for predicting S_d.
4. For Model I and II, since β, γ and n parameters did not show robust correlations (i.e. R>0.9) with D_{50} or C_u, the mean optimized β, γ and n were also evaluated as shown in Fig. 3-8(b), 3-8(c) and 3-9(b). With readily available correlations, several scenarios to predict β, γ and n parameters were developed in Table 3-3. These scenarios were then evaluated with other predicted parameters calculated in step 1 through 3. Two different ways of predicting S_c from step 2 were also combined into three scenarios for evaluation. The coefficient of determination (R^2) used to access overall goodness of curve fitting was calculated for each scenario. The results indicate that the difference between these

scenarios is not significant. Thus, the simplest way to directly use mean S_c, β, γ and n parameters is suggested for predicting S_c, β, γ and n (i.e. S_c = 0.098, β = 1.44, γ = 14.39 and n = 4.19).

Fig. 3-10 displays the measured TCDC fitted with the predicted TCDC (dash line) using mean S_c, β, γ and n parameters in Model I and II for SP5. The results demonstrate that both predicted models have good match with the experimental results. For overall predicted results of nine sands, the average coefficients of determination (R^2) are 0.957 and 0.974 respectively for Model I and II, which indicates that the Model II has relatively better performance than Model I.

A series of previous models mentioned in background section have also been fitted with the experimental TCDCs to be compared with Model I and II in this study. Figure 3-11 provides the fitting results of all these models including Model I and II for SP5. For the fitting parameters, λ_{sat} and λ_{dry} were set to the averaged λ_{sat} and λ_{dry} between Model I and Model II for all these models. Additionally, other selected empirical parameters and relationships included κ = 3.55 for the Côté and Konrad (2005) model, α = 0.96 for the Lu *et al*. (2007) model, m_c = 0 for the Campbell *et al.* (1985, 2011) model, and β' = 2.8β and λ_{crit} = 0.58λ_{sat} for Likos (2013) model. Among these previous models, Hu *et al.* (2001) provides the best predict for SP5, but still underestimates λ for the initial flat regime. The Johansen (1975), Côté and Konrad (2005) and Lu *et al.* (2007) models underpredict λ over almost entire range of the degree of saturation. Campbell (1985, 2011) and Likos (2013) models provides generally good fit for the low saturation range (i.e., $S < S_c$).

Fig. 3-12 compares the averaged R^2 for all nine sands between six previous models and 2 current proposed models. The averaged R^2 are 0.957 and 0.974 for Model I and II, and the Model

II provides the best R^2 among all the models. The skewness of previous models is likely attributed to inaccurate empirical parameters and relationships.

3.6 SUMMARY AND CONCLUSIONS

A suite of natural sands was tested in this study to develop two new mathematical models for estimating the thermal conductivity of coarse-grained soils at room temperature. These two new models were proposed based on generalized observation of four different regimes existing in thermal conductivity dry-out curves (TCDCs). The two proposed models, Model I and II, include eight and five fitting parameters, respectively. Through best fitting Model I and II on measured TCDCs, the fitting parameters were optimized, and several potential correlations with soil physical parameters were observed. The most notable correlations were found between S_c and S_r, and between S_b and D_{50}. Other fitting parameters, such as γ, β and n, did show acceptable but not robust correlations with D_{50} and C_u. Examining the correlations for γ, β and n with soil physical parameters (e.g., D_{50}, D_{10}, C_u, fines content) through a larger database should be considered in future work.

Using the mean values of γ, β and n, TCDCs were predicted with Model I and II for nine sands. The averaged coefficients of determination (R^2) are 0.957 and 0.974 for predicted Model I and II, respectively. This indicates that the predicted TCDCs demonstrate a good match over the full range of saturation for both Model I and II because these two models successfully captured the observed regimes. Additionally, predicted TCDCs with Model I and II were compared to previous models for TCDC, and Model II have the best performance among all the models.

3.7 NOTATION

The following symbols are used in this chapter:

C_c	=	coefficient of curvature
C_u	=	coefficient of uniformity
D_{10}	=	grain size at 10% finer by mass
D_{50}	=	median grain size by mass
e	=	void ratio
g	=	empirical weighing factor in Campbell (1985, 2011) model
G_s	=	specific gravity of soil solids
K_e	=	Kersten's number
m_c	=	clay fraction in soil by mass
n	=	porosity, van Genuchten (1980) fitting parameter, and fitting parameter in Model II, respectively
R	=	correlation coefficient
R^2	=	coefficient of determination
S	=	degree of saturation
S_b	=	saturation at lower limit of the initial flat regime (regime I)
S_c	=	saturation at sharp transition in TCDC
S_d	=	saturation where thermal conductivity levels off to minimum.
S_r	=	residual saturation
α	=	van Genuchten (1980) fitting parameter, and empirical parameter in Lu *et al*. (2007) model, respectively
β	=	fitting parameter in Model I, SWCC fitting parameter at low suction in Likos (2013) model, respectively
β'	=	SWCC fitting parameter at high suction in Likos (2013) model
γ	=	fitting parameter in Model I
κ	=	empirical parameter in Côté and Konrad (2005) model
λ	=	thermal conductivity
λ_{crit}	=	thermal conductivity at sharp transition in TCDC used in Likos (2013) model
λ_c	=	thermal conductivity at sharp transition in TCDC used in Model I
λ_{sat}	=	thermal conductivity at full saturation
λ_{dry}	=	thermal conductivity at dry conditions
θ	=	volumetric water content
θ_{sat}	=	saturated volumetric water content
θ_o	=	cutoff volumetric water content used in Campbell (1985, 2011) model
ψ	=	soil suction
ψ_b	=	soil suction at air-entry, Brooks and Corey (1964) fitting parameter
ψ_{crit}	=	soil suction at sharp transition in TCDC

3.8 REFERENCES

ASTM D 2487. (2011). "Standard Practice for Classification of Soils for Engineering Purposes (Unified Soil Classification System)."

ASTM D 4318-10. (2010). "Standard Test Methods for Liquid Limit, Plastic Limit, and Plasticity Index of Soils."

ASTM D 854-10. (2010). "Standard Test Methods for Specific Gravity of Soil Solids by Water Pycnometer."

ASTM D 6836-02. (2008). "Standard Test Methods for Determination of the Soil Water Characteristic Curve for Desorption Using Hanging Column, Pressure Extractor, Chilled Mirror Hydrometer, or Centrifuge."

ASTM D 422-63. (2007). "Standard Test Method for Particle-Size Analysis of Soils."

Bareither, C. A., Edil, T. B., Benson, C. H., and Mickelson, D. M. (2008). "Geological and Physical Factors Affecting the Friction Angle of Compacted Sands." *Journal of geotechnical and geoenvironmental engineering*, *134*(10), 1476-1489.

Brandl, H. (2006). "Energy Foundations and Other Thermo-Active Ground Structures." Geotechnique, 56(2), 81–122.

Brandon, T.L., Mitchell, J.K., and Cameron, J.T. (1989). "Thermal Instability in Buried Cable Backfills." *J. of Geotechnical Engineering*, ASCE, 115(1), 38-55.

Brandon, T.L., and Mitchell, J.K. (1989). "Factors Influencing Thermal Resistivity of Sands." *Journal of Geotechnical Engineering*, Vol. 115 (12): 1683-1698.

Brooks, R.H. and Corey, A.T. (1964). "Hydraulic Properties of Porous Media,"Hydrology Paper No. 3, Colorado StateUniv., Fort Collins, CO.

Campbell, G. S. (2011), "Producing Thermal Dryout Curves for Buried Cable Applications," Application Note 13994-01 AN, DecagonDevices, Inc., Pullman, WA.

Campbell, G.S., Jungbauer, J.D., Bidlake, W.R., and Hungerford, R.D. (1994). "Predicting the Effect of Temperature on Soil Thermal Conductivity." *Soil Science*, 158(5), 307-313.

Campbell, G. S. (1985). *Soil Physics with BASIC: Transport Models for Soil-Plant Systems* (Vol. 14). Elsevier Science

Côté, J., & Konrad, J. M. (2009). Assessment of Structure Effects on the Thermal Conductivity of Two-Phase Porous Geomaterials. *International Journal of Heat and Mass Transfer*, *52*(3), 796-804.

Côté, J., and Konrad, J. M. (2005). "A Generalized Thermal Conductivity Model for Soils and Construction Materials." *Canadian Geotechnical Journal*, *42*(2), 443-458.

de Vries, D.A. (1963). Thermal Properties of Soils. *Physics of Plant Environment*. W.R. van Wijk (ed.). North Holland Pub. Co. Amsterdam: 210-235.

Fan, R., Jiang, Y., Yao, Y., Shiming, D., and Ma, Z. (2007). "A Study on the Performance Of a Geothermal Heat Exchanger under Coupled Heat Conduction and Groundwater Advection." *Energy*, *32*(11), 2199-2209.

Farouki, O. T. (1981). *Thermal Properties of Soils* (No. CRREL-MONO-81-1). COLD REGIONS RESEARCH AND ENGINEERING LAB HANOVER NH.

Guymon, G. L., Berg, R. L., and Hromadka, T. V. (1993). *Mathematical Model of Frost Heave and Thaw Settlement in Pavements* (No. CREEL-93-2). COLD REGIONS RESEARCH AND ENGINEERING LAB HANOVER NH.

Hopmans, J.W., and Dane, J.H. (1986). "Thermal Conductivity of Two Porous Media as a Function of Water Content, Temperature, and Density." *Soil Science Society of America Journal*, Vol. 142 (4): 187-195.

Hu X-J, Du J-H, Lei S-Y, Wang B-X (2001) A Model for the Thermal Conductivity of Unconsolidated Porous Media Based on Capillary Pressure-Saturation Relation. Int J Heat Mass Transf 44:247–251

Johansen, O. (1975). "Thermal Conductivity of Soils." Ph.D. thesis, Institute for Kjoleteknikk, Trondheim, Norway.

Kersten, M. S. (1949). *LABORATORY RESEARCH FOR THE DETERMINATION OF THE THERMAL PROPERTIES OF SOILS.* MINNESOTA UNIV MINNEAPOLIS ENGINEERING EXPERIMENT STATION.

Likos, W. (2013). "Modeling Thermal Conductivity Dryout Curves from Soil-Water Characteristic Curves." *J. Geotech. Geoenviron. Eng.* , 10.1061/(ASCE)GT.1943-5606.0001078 , 04013056.

Likos, W. J., Olson, H. S., and Jaafar, R. (2012). "Comparison of Laboratory Methods for Measuring Thermal Conductivity of Unsaturated Soils." *GeoCongress 2012*

Lu S, Ren TS, Gong YS, Horton R (2007) An Improved Model for Predicting Soil Thermal Conductivity from Water Content at Room Temperature. Soil Sci Soc Am J 71:8–14

Sakaki, T., Limsuwat, A., Smits, K. M., and Illangasekare, T. H. (2008). "Empirical Two-Point A-Mixing Model for Calibrating the ECH2O EC-5 Soil Moisture Sensor in Sands." *Water Resources Research*, *44*(4).

Shelton, J. (1975). Underground Storage of Heat in Solar Heating Systems. *Solar Energy*, *17*(2), 137-143.

Smits, K. M., Sakaki, T., Limsuwat, A., and Illangasekare, T. H. (2010). "Thermal Conductivity of Sands under Varying Moisture and Porosity in Drainage - Wetting Cycles." *Vadose Zone Journal*, *9*(1), 1-9.

Smits, K. M., Sakaki, T., Limsuwat, A., and Illangasekare, T. H. (2009). "Determination of the Thermal Conductivity of Sands under Varying Moisture, Drainage/Wetting, and Porosity Conditions: Applications in Near-Surface Moisture Distribution Analysis." Proc., AGU Hydrology Days 2009.

van Genuchten, M.T., 1980, "A Closed Form Equation for Predicting the Hydraulic Conductivity of Unsaturated Soils," *Soil Science Society of America Journal*, Vol. 44, 892-898.

3.9 TABLES

Table 3-1. Properties summary for nine sands

Sample	USCS	D_{50} (mm)	D_{10} (mm)	C_u	C_c	Fines (%)	G_s
SP1	SP	0.38	0.18	2.4	1.0	0.6	2.65
SP2	SP	0.29	0.18	1.8	0.9	1.8	2.68
SP3	SP	0.34	0.12	3.4	1.6	4.8	2.68
SP4	SP	0.50	0.13	4.8	1.5	2.0	2.72
SP5	SP	0.22	0.15	1.6	1.0	1.1	2.66
SP7	SP	0.50	0.26	2.2	1.0	1.8	2.65
SP-SM8	SP-SM	0.19	0.08	2.6	1.3	7.4	2.70
SM1	SM	0.11	0.05	2.6	1.1	20.8	2.68
SM2	SM	0.13	0.05	3.2	1.0	19.9	2.75

Table 3-2. Summarized best-fitting parameters for nine sands

Sample	Model I Parameters									Model II Parameters					VG Paramters		
	λ_{sat}	λ_{dry}	S_d	S_c	S_b	γ	β	γ/β	λ_c	λ_{sat}	λ_{dry}	n	S_d	S_b	α	n (VG)	S_r
SP1	2.70	0.49	0.014	0.078	0.611	18.72	1.89	9.92	1.69	2.70	0.54	4.23	0.026	0.690	0.41	3.52	0.066
SP2	2.43	0.50	0.007	0.116	0.863	11.19	0.94	11.91	1.72	2.43	0.57	4.51	0.013	0.912	0.25	4.72	0.085
SP3	2.30	0.59	0.027	0.165	0.725	7.82	1.12	6.99	1.67	2.30	0.59	3.78	0.027	0.723	0.27	3.05	0.208
SP4	1.72	0.35	0.001	0.128	0.453	6.87	1.54	4.45	1.22	1.72	0.44	3.56	0.026	0.473	0.85	2.84	0.051
SP5	2.43	0.40	0.025	0.098	0.696	15.38	1.51	10.18	1.52	2.43	0.41	4.19	0.038	0.800	0.20	4.77	0.072
SP7	2.62	0.37	0.006	0.066	0.588	20.10	2.01	10.02	1.57	2.63	0.39	3.96	0.018	0.683	0.41	3.58	0.041
SP-SM8	2.45	0.38	0.011	0.058	0.632	24.17	1.62	14.94	1.52	2.47	0.38	4.52	0.019	0.768	0.17	3.56	0.039
SM1	2.20	0.48	0.016	0.109	0.745	11.02	1.10	9.99	1.50	2.22	0.53	4.91	0.037	0.880	0.10	3.99	0.087
SM2	2.17	0.38	0.002	0.066	0.773	14.30	1.24	11.54	1.29	2.18	0.42	4.03	0.010	0.908	0.12	3.13	0.054
Mean	2.33	0.44	0.012	0.098	0.676	14.39	1.44	9.99	1.52	2.34	0.47	4.19	0.024	0.760	0.31	3.68	0.078
STD	0.29	0.08	0.009	0.035	0.120	5.80	0.37	2.96	0.17	0.29	0.08	0.41	0.010	0.139	0.23	0.69	0.052

Table 3-3. Comparison of three scenarios to predict *β*, *γ* and *n* parameters

Scenario	Model I	R^2	Model II	R^2
1	S_c, β, γ = mean	0.957	n = mean	0.974
2	S_c vs. S_r; β = mean; γ/β vs. D_{50}	0.946	n vs. D_{50}	0.977
3	S_c vs. S_r; β =mean; γ/β vs. C_u	0.952	n vs. C_u	0.972

3.10 FIGURES

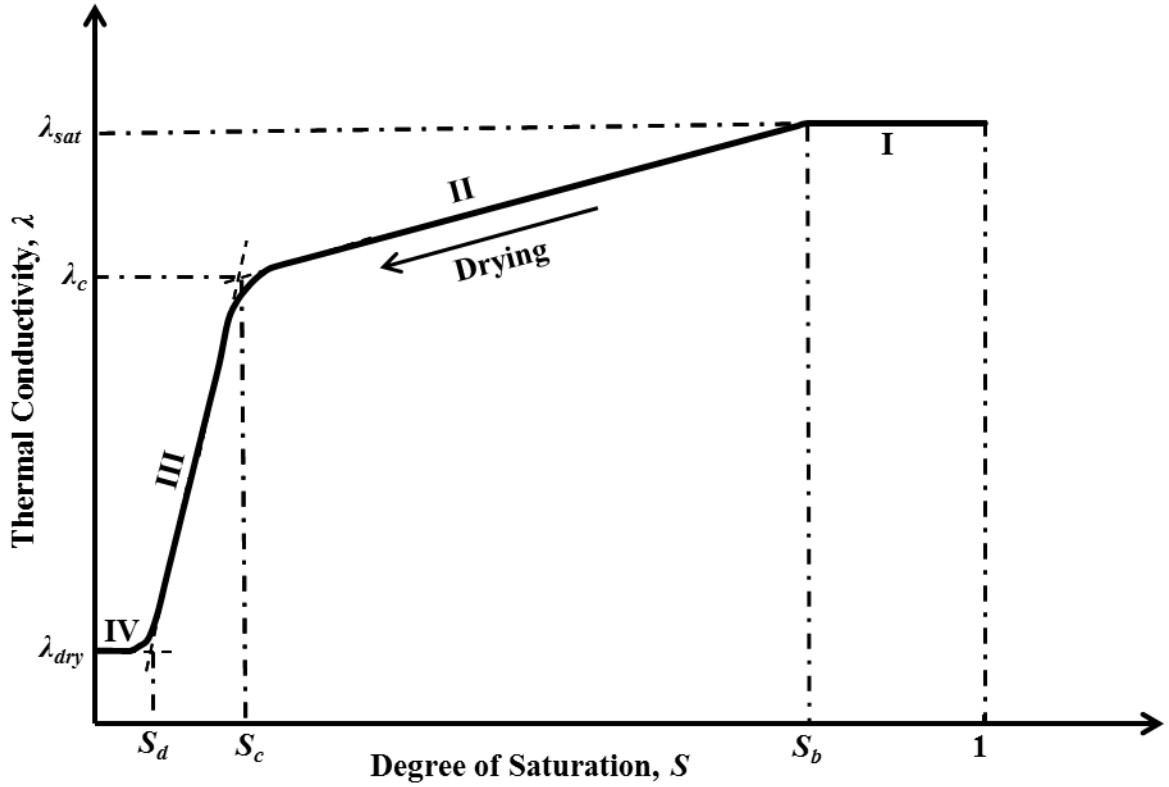

Figure 3-1. Typical thermal conductivity dry-out curve (TCDC) for coarse grained soil

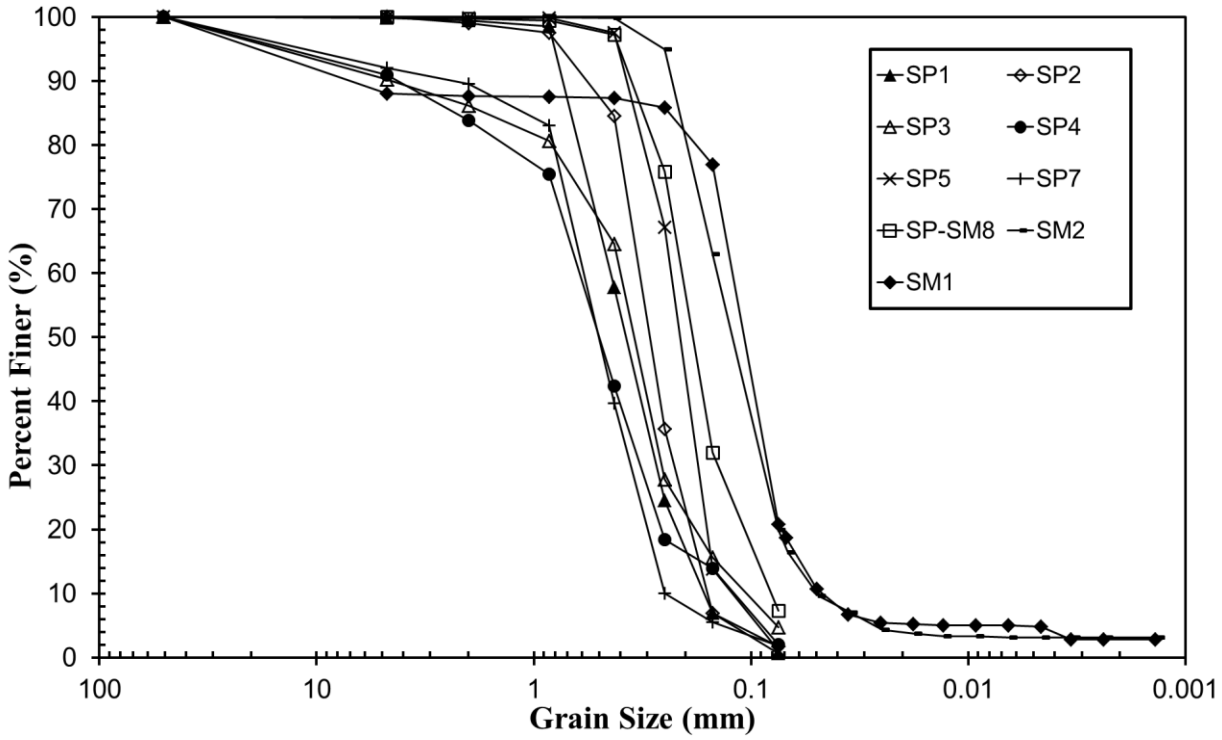

Figure 3-2. Grain size distribution for nine sands

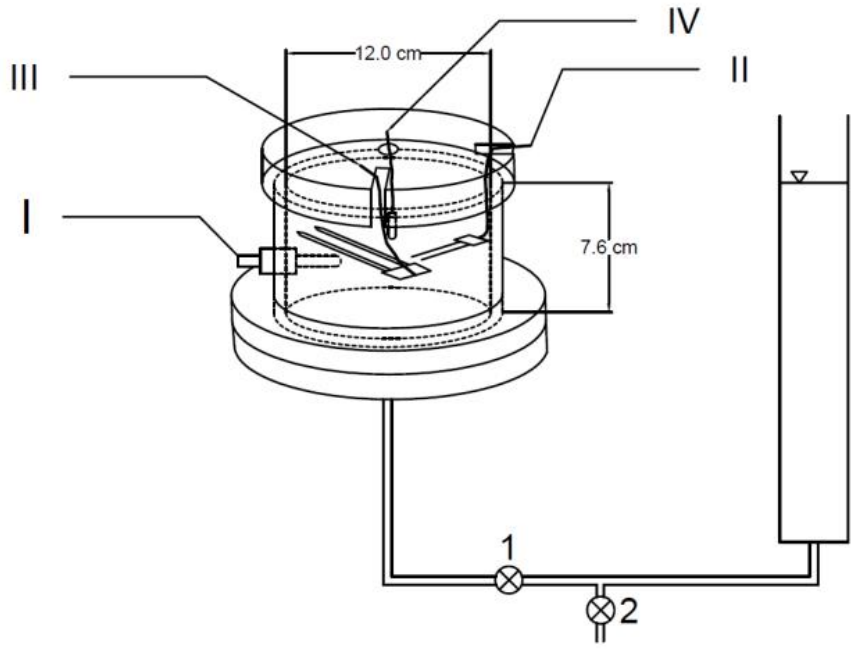

Figure 3-3. Schematic of modified hanging column apparatus

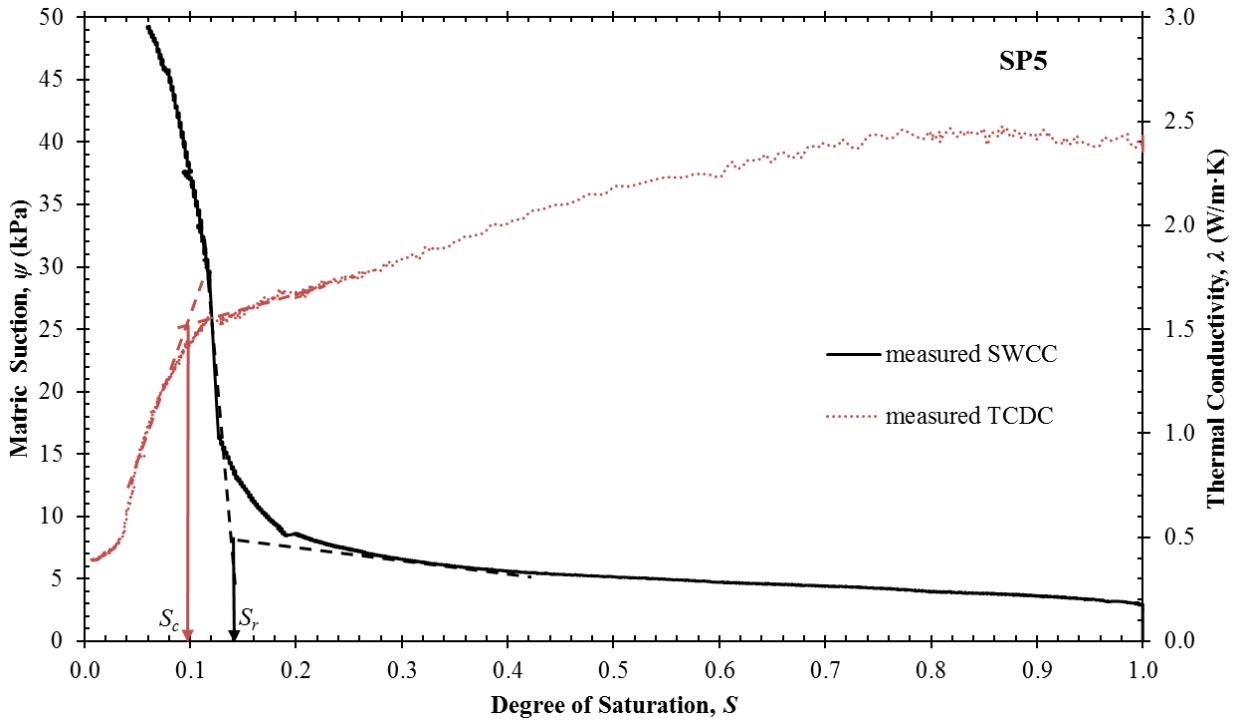

Figure 3-4. Measured TCDC and SWCC for SP5

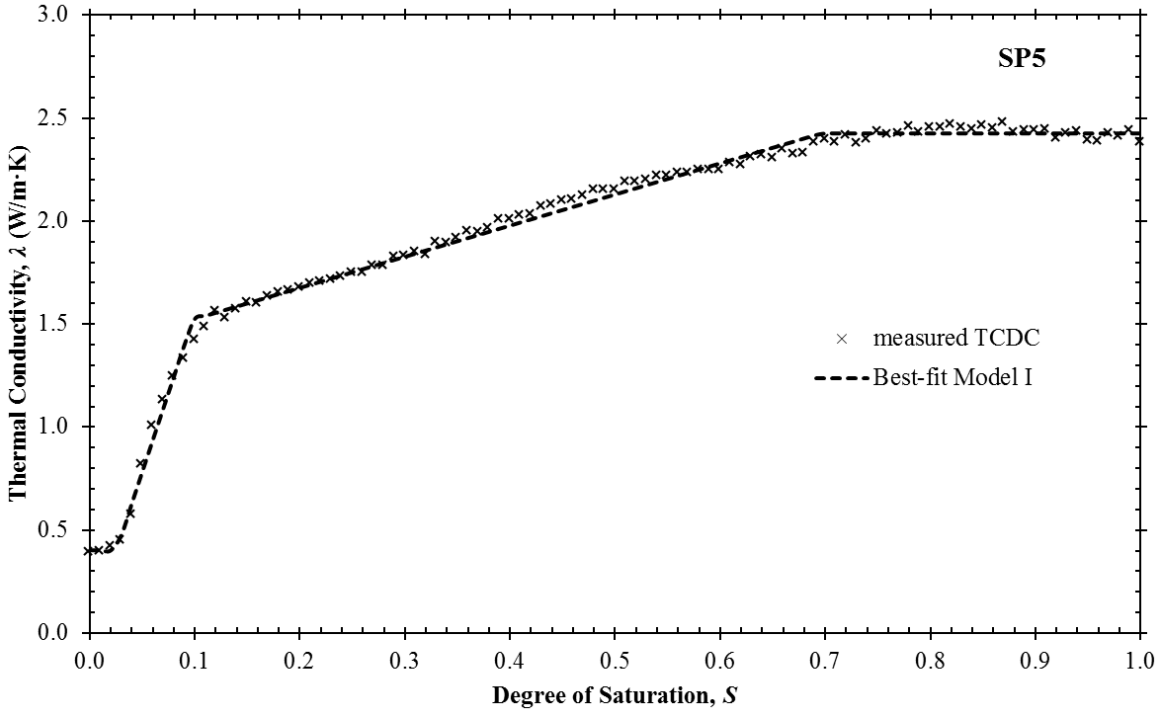

(a)

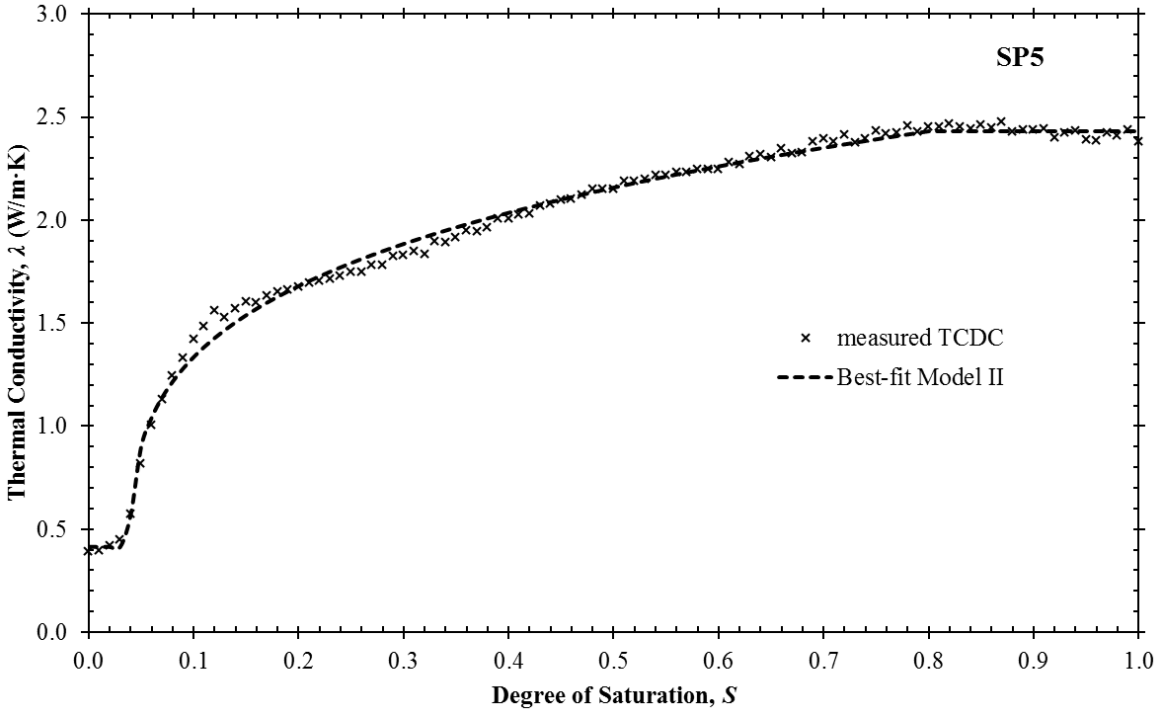

(b)

Figure 3-5. Measured TCDCs and best-fit TCDCs with (a) Model I and (b) Model II for SP5

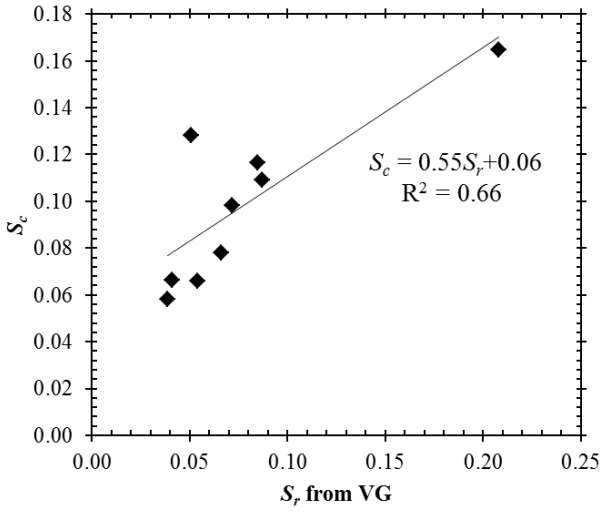

(a)

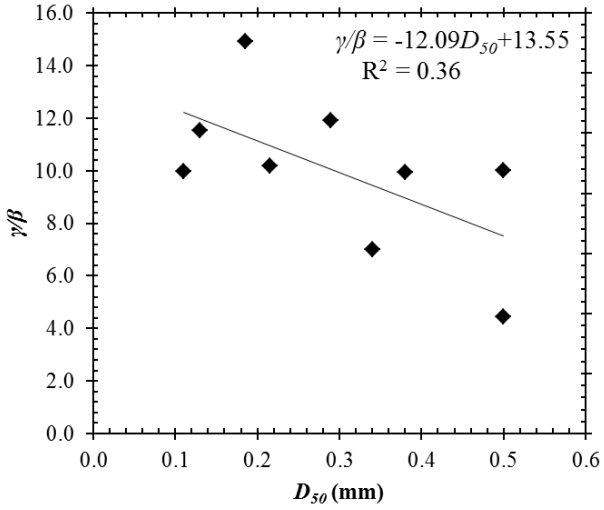

(b)

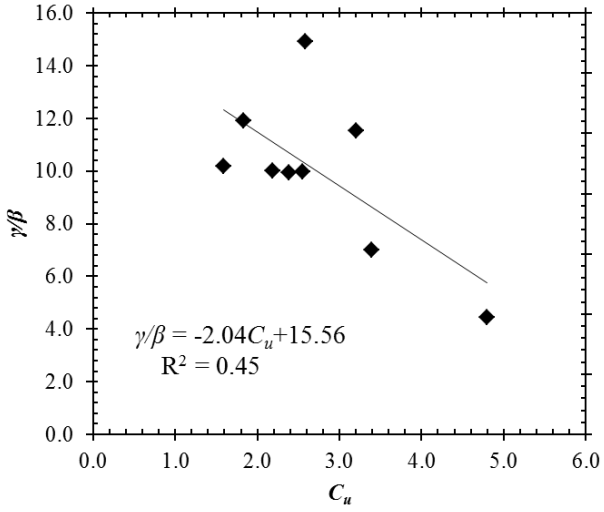

(c)

Figure 3-6. Correlations between (a) S_c and S_r from VG; (b) γ/β and D_{50}; (c) γ/β and C_u for Model I

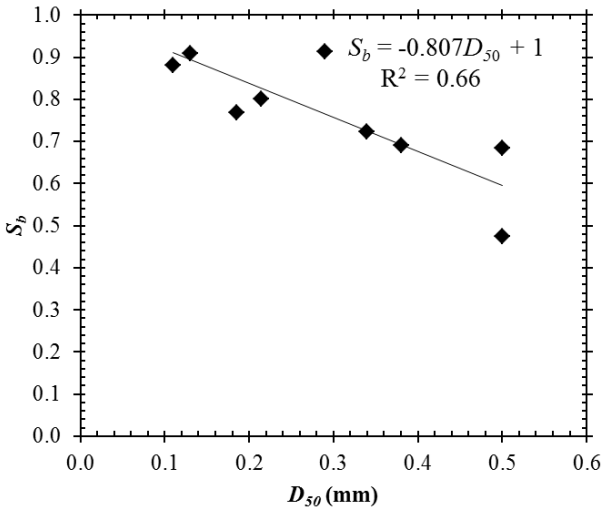

(a)

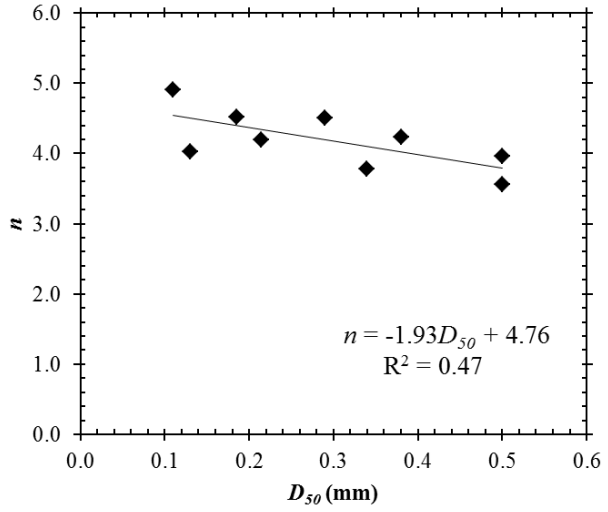

(b)

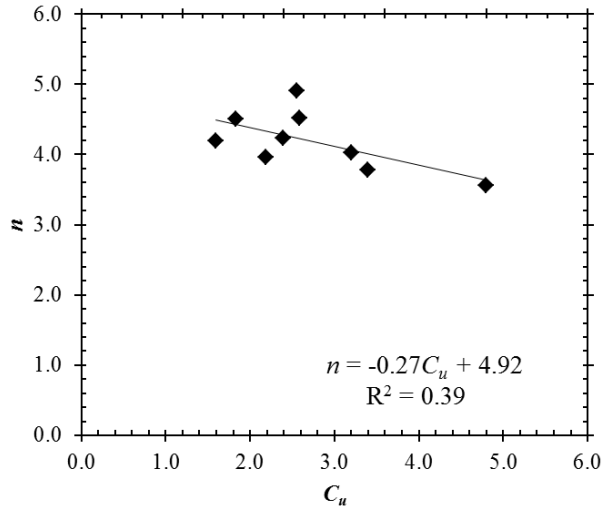

(c)

Figure 3-7. Correlations between (a) S_b and D_{50}; (b) n and D_{50}; (c) n and C_u for Model II

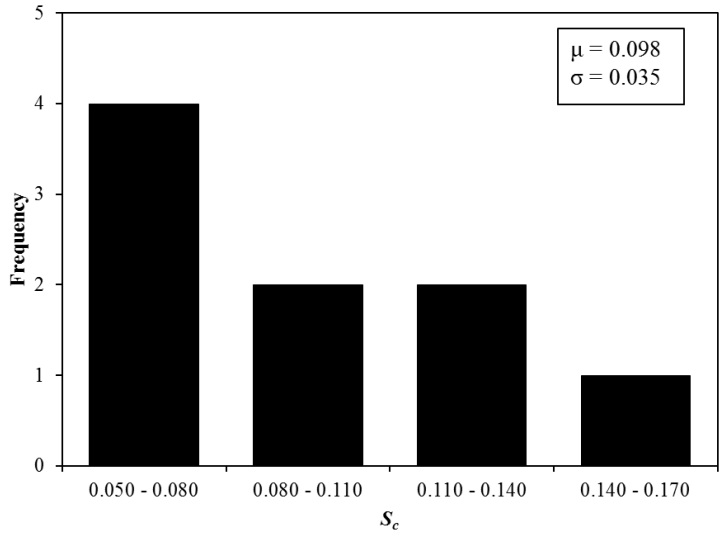

(a)

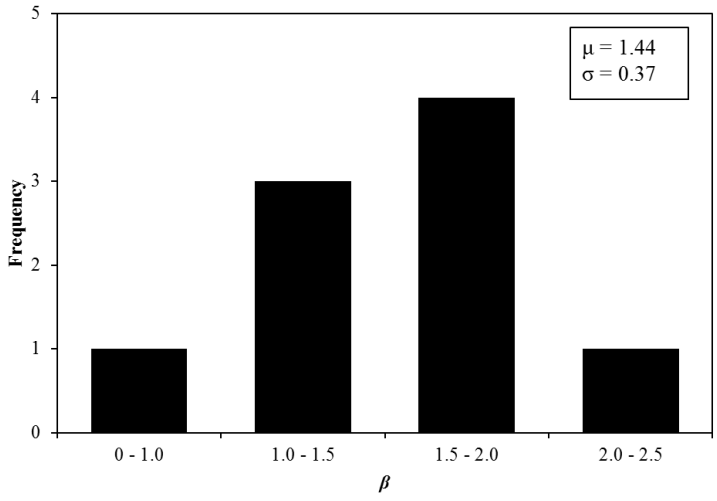

(b)

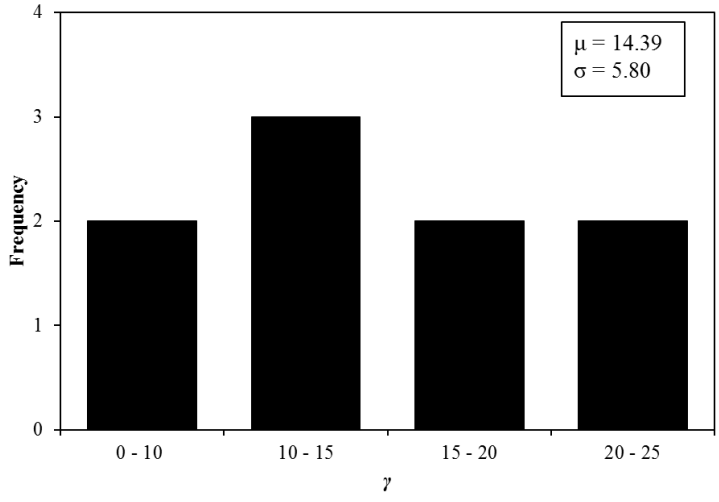

(c)

Figure 3-8. Histograms for S_c, β, and γ with mean and standard deviation values

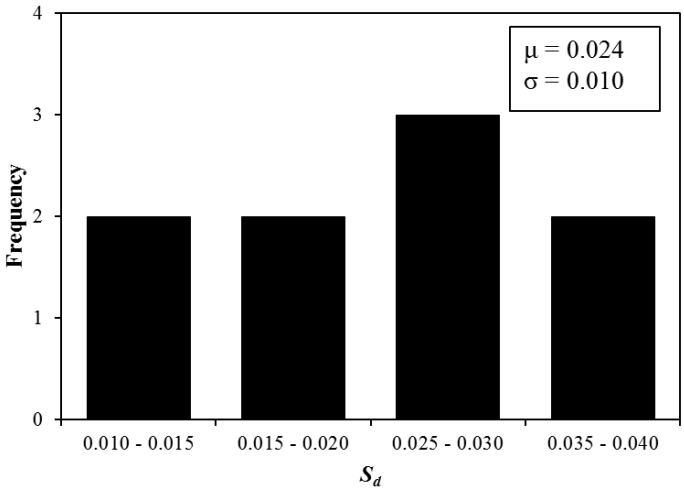

(a)

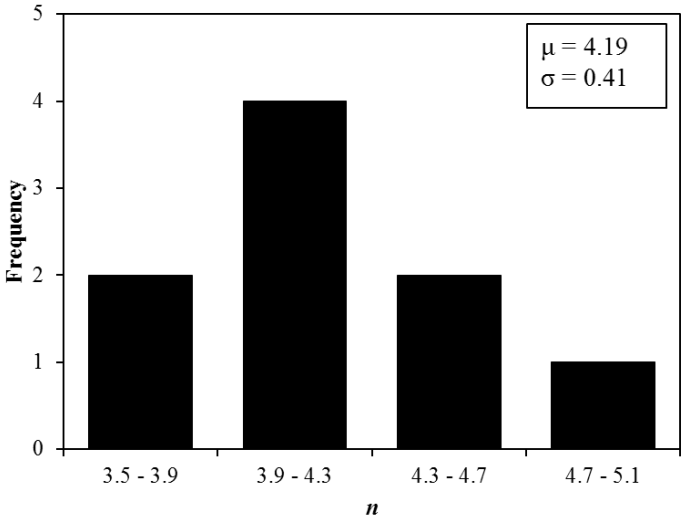

(b)

Figure 3-9. Histograms for S_d and *n* with mean and standard deviation values

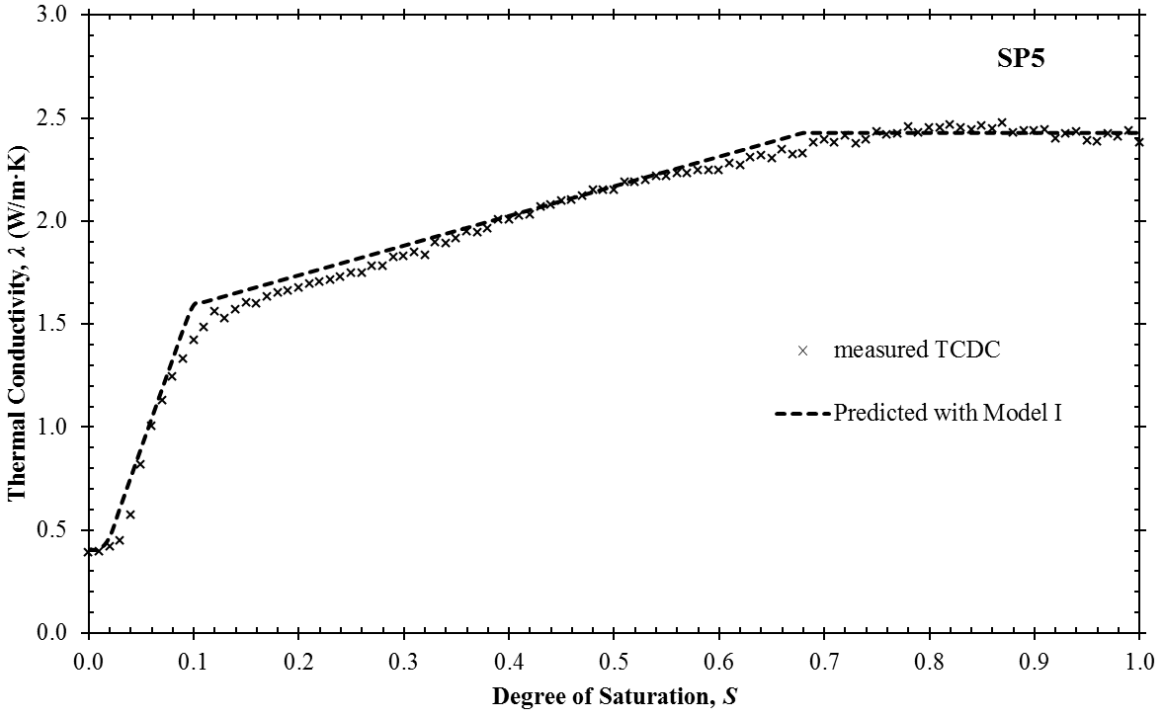

(a)

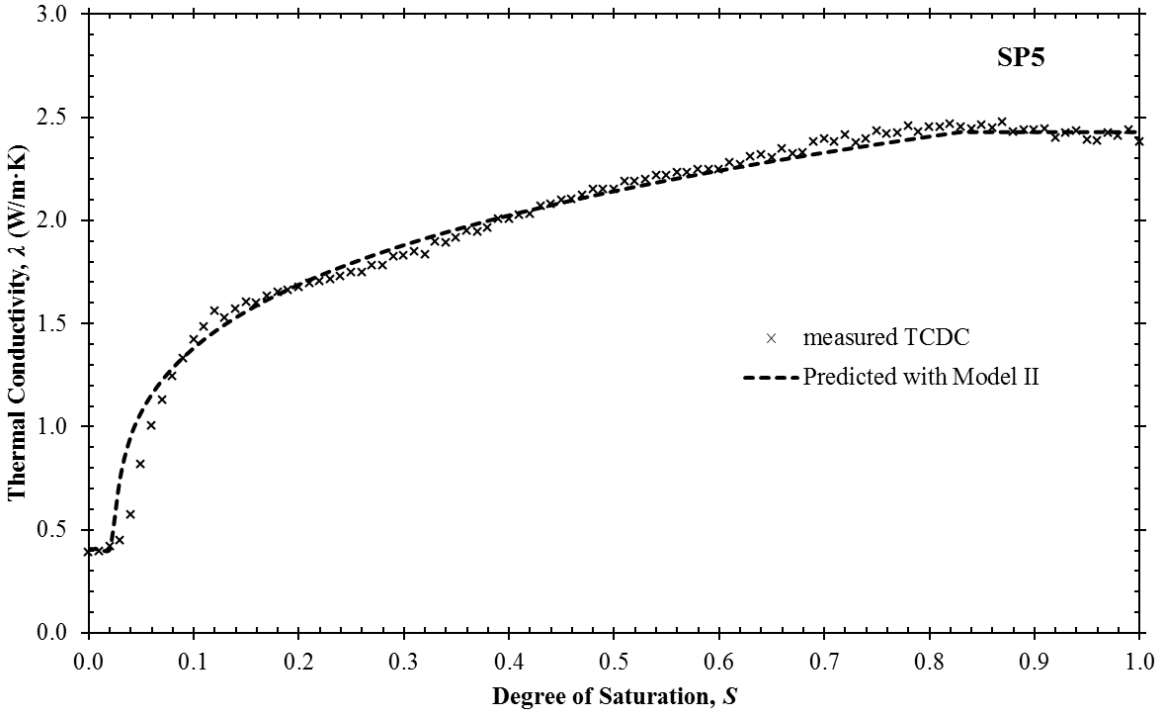

(b)

Figure 3-10. Measured TCDCs and predicted TCDCs with (a) Model I and (b) Model II for SP5

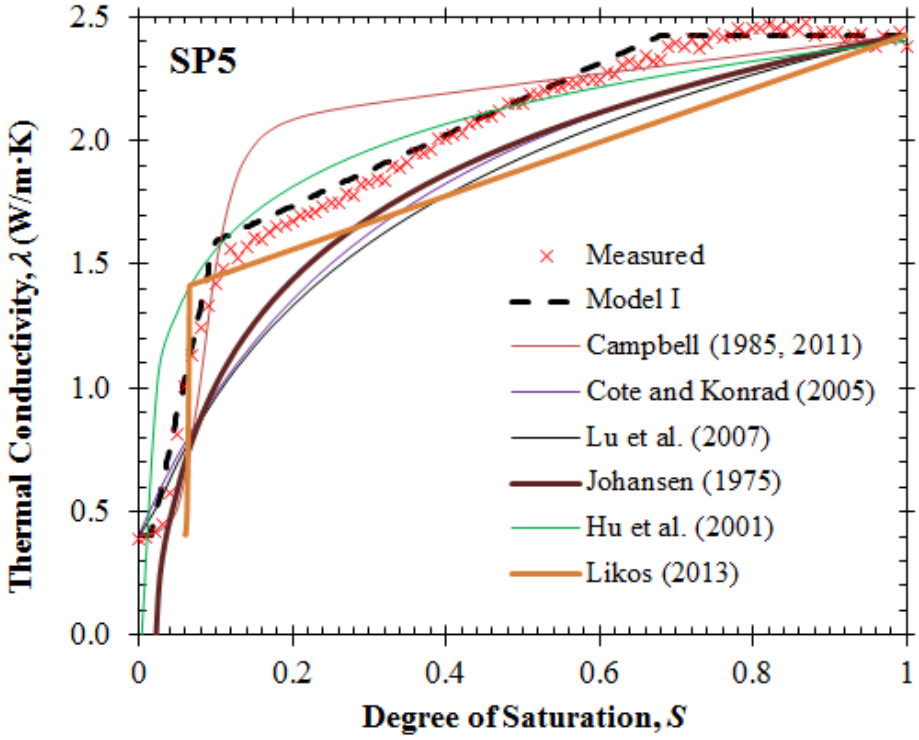

(a)

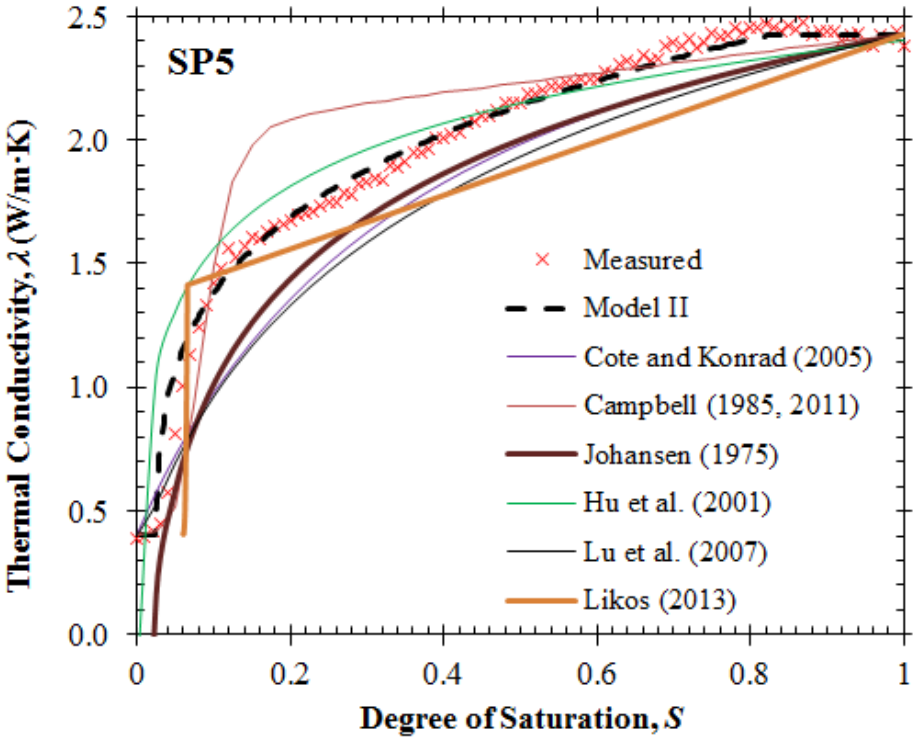

(b)

Figure 3-11. Measured and modeled TCDCs using various models for SP5

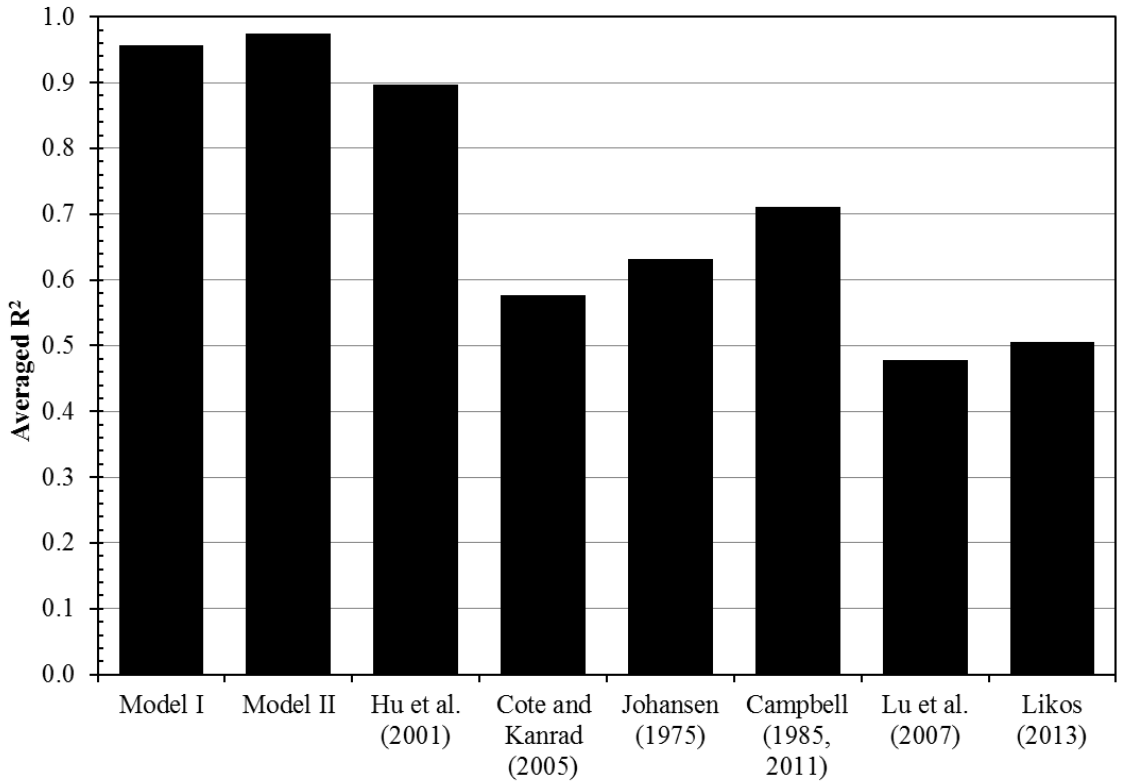

Figure 3-12. Comparison of averaged R^2 among several models

CHAPTER FOUR

CONCLUSIONS AND RECOMMENDATIONS

Based on the findings in Chapters 2 and 3, several key conclusions and recommendations are made as the following:

1) The modified hanging column method is recommended for producing TRDCs or TCDCs because it produces the most robust and well-defined curves.
2) Among three laboratory methods, the multiple-specimen method requires the least amount of time (i.e. 1 day) to produce TRDCs or TCDCs. Thus, the multiple-specimen method could be used for time-sensitive tests for TRDCs or TCDCs.
3) The modified hanging column method slightly overestimates the thermal resistivity of soils when soils remain in primary drainage period compared to the other two methods. This is potentially due to forced convection caused by water movement and free convection caused by larger heat pulse created by SH-1 dual needle sensor. More detailed analysis should be considered regarding this potential limitation in future study.
4) Two new proposed models demonstrate better prediction performance compared to the models in previous studies.
5) The second model (Model II) with a non-linear segment is recommended for general application because it has fewer fitting parameters than the first model (Model I).
6) Correlations between the model fitting parameters (e.g. γ, β, n) and soil physical parameters (e.g. D_{50}, D_{10}, C_u, fines content) are not strong. More comprehensive study with a larger database on these correlations should be considered in future work.

CHAPTER FIVE

APPENDIX - A
EFFECTS OF CONSTRAINTS ON VAN GENUCHTEN PARAMETERS FOR MODELING SOIL-WATER CHARACTERISTIC CURVES

ABSTRACT: Water retention data for a suite of predominantly sandy soils are analyzed to quantify the effects of two constraints commonly applied to van Genuchten's (1980) three-parameter model for the soil-water characteristic curve (SWCC). Systematic effects are observed. Constraining either the symmetry parameter (m) to m = 1-1/n or residual saturation (S_r) to zero results in values for the air-entry parameter α that average about 25% to 30% different than if no constraints are applied. The m = 1-1/n constraint forces values of the pore size distribution parameter n to fall within a narrow range (~1.5 < n < ~4.0), whereas n values using independent m and n are more variable and can be as large as 35. The m = 1-1/n constraint produces best-fit residual saturation values that are about 0.02 higher than values without the constraint. These differences are not insignificant and should be considered when adopting existing or new pedotransfer functions for estimating water retention behavior of unsaturated soils from more easily measured properties.

INTRODUCTION

The soil-water characteristic curve (SWCC) defining the relation between degree of saturation (S) and suction (ψ) is a fundamental element of unsaturated soil mechanics required to characterize essentially all aspects of unsaturated soil behavior. Applying the SWCC in analytical and numerical frameworks for predicting or interpreting unsaturated soil behavior typically requires that the SWCC, which is most often determined from discrete experimental measurements, be expressed in continuous mathematical form. A large number of parametric models for representing the SWCC have thus been proposed, most of which are used to best fit

experimentally determined water retention data for interpolation or extrapolation over some range of interest. In the geotechnical engineering community, these models most notably include those proposed by Brooks and Corey (1964), van Genuchten (1980), and Fredlund and Xing (1994). Detailed reviews and analyses of these and other models have been provided by a number of authors (*e.g.*, Leong and Rahardjo, 1997; Sillers *et al.*, 2001; Lu and Likos, 2004).

The emphasis of this note is on van Genuchten's (VG) commonly adopted three-parameter SWCC model in the form:

$$S_e = \frac{S - S_r}{1 - S_r} = \left[1 + (\alpha\psi)^n\right]^{-m} \tag{17}$$

where S_r is residual saturation, S_e is effective saturation, ψ is matric suction (kPa), α is a parameter having inverse units of suction (kPa^{-1}) and related to the inverse of the air-entry pressure, and n and m are dimensionless fitting parameters. The n parameter is related to pore size distribution and is generally larger for soils having narrow pore or grain size distribution and a corresponding flat SWCC. The m parameter is related to the overall symmetry of the SWCC. Effective saturation (S_e) normalizes degree of saturation between zero at $S = S_r$ and one at $S = 1$. Fitting the VG model through measured S-ψ data is usually achieved by nonlinear least-squared optimization of α, n, m, and S_r to minimize the residual sum of squares of observed and fitted saturation, typically using one of several available algorithms or multivariable solvers embedded in commercial spreadsheet packages (*e.g.*, van Genuchten *et al.*, 1991; Leij *et al.*, 1996).

The purpose of this study is to quantitatively examine the effects of two constraints often imposed on the VG parameters during curve fitting, namely $m = 1\text{-}1/n$ and $S_r = 0$. The study is motivated by the need to more effectively quantify uncertainty inherent in the variety of "pedotransfer" (PTF) approaches available for indirectly estimating SWCC parameters such as

α, n, and m by empirical correlation with more easily measured soil properties such as grain size, grain size distribution, and porosity (*e.g.*, Rawls and Brakensiek, 1985; van Genuchten *et al*. 1992; Wösten *et al*., 2001; Vereecken *et al*., 2010). As noted by Schaap and Leij (1998) and Zapata *et al*. (2000), the quality of such correlations depends heavily on the quality of the empirical database used to fit and test the correlations. We argue here that in addition to the quality of the database, the constraints adopted in SWCC fitting procedures used to develop the correlations, which are often not known or specified, may also be important to consider. Emphasis is placed on the VG constraints $m = 1\text{-}1/n$ and $S_r = 0$ for coarse-grained soils for two reasons: (*i*) because these constraints are commonly adopted in practice, and (*ii*) because correlations between VG fitting parameters and grain size parameters most relevant for coarse soils (*e.g.*, d_{50}, d_{10}, C_u, C_c) have found some success (*e.g.*, Yang *et al.* 1994; Benson *et al*, 2014). Despite this success, however, there remains substantial and largely unexplained variability (Schaap and Leij, 1998; Vereeken *et al*., 2010).

VAN GENUCHTEN PARAMETER CONSTRAINTS

In deriving closed-form solutions for unsaturated hydraulic conductivity, van Genuchten (1980) presented two constraints that explicitly link the symmetry parameter m to the pore size distribution parameter n. The first was derived from consideration of Mualem's (1976) capillary model and is in the form $m = 1 - 1/n$ ($n > 1$, $0 < m < 1$). The second was derived from consideration of Burdine's (1953) capillary model and is in the form $m = 1 - 2/n$ ($n > 2$, $0 < m < 1$). While both constraints provide benefit by reducing the number of unknowns for parameter optimization and facilitating closed-form analytical solutions, they also reduce the VG model flexibility and can lead to poor representation for soils having distinct air-entry regions (Kosugi

et al., 2002). The m = 1-1/n constraint is more widely adopted in geotechnical practice and is the focus of subsequent analysis.

The second constraint (S_r = 0) arises from uncertainty surrounding the concept of residual saturation. While the term "residual" saturation has some physical meaning in the sense that it can be used to describe soil pore water at low saturation, such as water in the form of disconnected menisci and adsorbed films (*e.g.*, Luckner, 1989; Nimmo, 1991; Vanapalli *et al*., 2008), the water content of unsaturated soil theoretically goes to zero as suction increases to infinity. Non-zero values of S_r in models such as VG result in some finite minimum degree of saturation that unrealistically becomes asymptotic as suction increases to infinity (Figure 5-1). This is not only an incorrect representation of soil water retention at high suction, but can also lead to convergence and stability issues in numerical simulations (Webb, 2000). Observation of an "irreducible" or residual saturation is often the case in experimental SWCC data obtained by gravity drainage, hanging column, or air pressure extraction tests, but this is due to experimental limitations resulting primarily from loss of continuity in the liquid water phase at low saturation (*e.g.*, Gee *et al*., 2002; Bittelli and Flury; 2009). Selection of a finite and non-zero S_r value is merely for the convenience of fitting the observed experimental data (Kosugi *et al*., 2002). SWCC formulations that incorporate finite values of suction at zero water content, rather than finite values of water content at infinite suction, are more physically representative in this regard (*e.g.*, Fredlund and Xing, 1994; Webb, 2000; Schneider and Goss, 2012; Revil and Lu, 2013).

Figure 5-1 illustrates the SWCC for typical silty sand and corresponding VG models found to best fit the experimental data. Model fitting parameters were obtained under three conditions: (*i*) using no parameter constraints (*i.e.*, independent α, n, m, and S_r); (*ii*) using independent α, n, and S_r with the constraint $m = 1 - 1/n$; and (*iii*) using independent α and n with

the constraints $m = 1 - 1/n$ and $S_r = 0$. Corresponding parameters for each case are summarized on Table 5-1. Several observations can be made from this example: (*i*) the flexibility gained by not applying parameter constraints results in the most accurate representation of the data; (*ii*) applying the $m = 1 - 1/n$ constraint alone results in lower α, lower n, and higher S_r compared with the case of no constraints; (*iii*) applying the $S_r = 0$ constraint alone results in higher α and substantially higher n compared with the case of no constraints; and (*iv*) applying both the $m = 1 - 1/n$ and $S_r = 0$ constraints results in lower α and lower n compared with the case of no constraints. It follows that if one develops a pedotransfer function to relate, for example, n to C_u for sandy soils, then the correlation may depend to some extent on the SWCC fitting constraints adopted to obtain the n parameters in the database queried for the correlation.

ANALYSIS APPROACH AND RESULTS

A database including SWCCs and grain size information for 44 coarse-grained (predominantly sand-sized) soils was analyzed to examine the generality of the above observations and to obtain correlations between VG fitting parameters obtained with and without applying the $m = 1\text{-}1/n$ and $S_r = 0$ constraints. Information for 33 of these soils was obtained from the UNSODA database (Leij *et al*., 1996). The remaining 11 soils were obtained and tested for grain size and water retention characteristics by the authors. All SWCC results corresponded to initial drainage paths. Median grain size (d_{50}) for the suite of materials ranged from 0.10 mm to 0.71 mm and averaged 0.32 mm. Percent fines ranged from less than 1% to 24% and averaged 10.6%. Coefficient of uniformity (C_u) ranged from 1.6 to 20.6 and averaged 5.3, indicating a wide range of poorly-graded and well-graded materials. Fourteen of the 44 soils (32%) classified according to the Unified Soil Classification System (USCS) as either SP-SM or SP-SC, 18 (40%) were SM or SC, nine (21%) were SP, and three (7%) were SW. Discrete water retention data for

each of the soils were best fit using the VG model implemented into a spreadsheet with parameter optimization using a multivariable solver to minimize the difference between modeled and measured saturations. Optimizations were conducted under the four constraint conditions noted above.

Figure 5-2 is a summary of results obtained for the α parameter. Figure 5-2a compares α values obtained with no parameter constraints (α_0) with values obtained using only the m = 1-1/n constraint [$\alpha_{(m=1-1/n)}$]. Figure 5-2b compares α_0 to values obtained using only the S_r = 0 constraint [$\alpha_{(Sr=0)}$]. Figure 5-2c compares α_0 to values obtained using the both the S_r = 0 and m = 1-1/n constraints [$\alpha_{(Sr=0;m=1-1/n)}$].

The air-entry parameter without constraints applied ranges from 0.09 kPa^{-1} to 2.41 kPa^{-1} and averages 0.50 kPa^{-1} for the suite of 44 soils. While there is some scatter, most α_0 values tend to cluster within a range from about 0.15 to 0.70. These values are slightly lower than results from the large database of Carsel and Parrish (1988), which indicates average α of 0.77 kPa^{-1} and 1.26 kPa^{-1} for soils similar to those examined here (classified according to the USDA textural classification as sandy loam and loamy sand, respectively).

Observation of Figure 5-2a indicates that applying the m = 1-1/n constraint results in a majority of points falling below the 1:1 correspondence line. The range of α for m = 1-1/n is from 0.10 kPa^{-1} to 1.28 kPa^{-1}, with an average of 0.41 kPa^{-1}. Applying the m = 1-1/n constraint results in an α value that is about 30% less on average than if the constraint is not applied. This is captured by the trendline constructed through the data on Figure 5-2a and the corresponding equation:

$$\alpha_{(m=1-1/n)} = 0.70(\alpha_0) \qquad (18)$$

Results on Figure 5-2b indicate that applying only the $S_r = 0$ constraint results in α values consistently higher than if the constraint is not applied. Values of $\alpha_{(Sr=0)}$ average about 25% higher than α_0, as described by:

$$\alpha_{(Sr=0)} = 1.25(\alpha_0) \tag{19}$$

If both constraints are applied concurrently (Figure 5-2c), the net effect is a value of α that averages about 15% lower than if no constraints are applied:

$$\alpha_{(Sr=0;m=1-1/n)} = 0.85(\alpha_0) \tag{20}$$

Figure 5-3 is a similar series of figures summarizing the effects of parameter constraints on the pore size distribution parameter *n*. With no constraints applied, n_0 for the suite of soils ranges from about one to 34, although most data points cluster within about one to seven. Applying the $m = 1\text{-}1/n$ constraint alone (Figure 5-3a) has a significant effect on the range and distribution of *n*. The constraint results in a narrower band of *n* (~1.5 < *n* < ~4.0) with an average of 3.15 and standard deviation of 1.05. This range is in reasonable agreement with the Carsel and Parrish (1988) database, which indicates average *n* of 1.89 and 2.28 for sandy loam and loamy sand, respectively. Unlike the case for the α parameter, however, there is no systematic correlation between the constrained *n* values and the unconstrained *n* values.

If the $S_r = 0$ constraint is applied alone (Figure 5-3b), $n_{(Sr=0)}$ is generally greater than n_0, and can be greater than 60 in extreme cases. If both constraints are applied (Figure 5-3c), the range of *n* reduces to an even narrower band than noted above with an average of 2.19 and standard deviation of 0.80. Because *n* and *m* are explicitly linked by the $m = 1\text{-}1/n$ constraint, this in turn creates a narrow band of *m* that averages 0.50 with a standard deviation of 0.14 for the suite of soils.

Figure 5-4 is a comparison of residual saturation if treated as an independent fitting parameter [$(S_r)_0$] with values obtained under the constraint m = 1-1/n. Applying the constraint results in S_r values greater than the unconstrained values in the majority of cases. $(S_r)_{(m=1-1/n)}$ averages about 0.02 greater than $(S_r)_0$, as described by:

$$(S_r)_{(m=1-1/n)} = (S_r)_0 + 0.02 \tag{21}$$

SUMMARY AND CONCLUSIONS

Empirical correlations were obtained for a suite of 44 predominantly sandy soils to quantify effects of the constraints m = 1-1/n and S_r = 0 on van Genuchten (1980) fitting parameters for the SWCC. The study is motivated by the need to more effectively quantify uncertainty in pedotransfer approaches commonly adopted for indirectly estimating the water retention and hydrologic properties of unsaturated soils in lieu of more time consuming and expensive experimental measurements. Applying either the m = 1-1/n constraint or S_r = 0 constraint results in values for the air-entry parameter α that are about 30% lower than or 25% higher than, respectively, the case when no parameter constraints are applied. Concurrently adopting both constraints results in α that averages about 15% less than if no constraints are applied. Applying the m = 1-1/n constraint forces values of the pore size distribution parameter n to fall within a relatively narrow range and residual saturation (S_r) values that average about 0.02 higher than without the constraint. These differences are not insignificant and should be considered when adopting existing or new pedotransfer functions for estimating water retention behavior of unsaturated soils.

REFERENCES

Benson, C.H., Chiang, I., Chalermyanont, T., and Sawangsuriya, A., 2014, "Estimating van Genuchten parameters α and n for clean sands from particle size distribution data," *ASCE GSP* 234-235.

Bittelli, M. and Flury, M., 2009, "Errors in water retention curves determined with pressure plates," *Soil Sci. Soc. Am. J.*, 73:1453-1460.

Brooks, R.H. and Corey, A.T., 1964, "Hydraulic properties of porous media," *Colorado State University, Hydrology Paper No. 3*, March.

Burdine, N.T., 1953, "Relative permeability calculation from pore size distribution data," *Trans. Am. Inst. Min. Eng*., 198: 71-78.

Carsel, R.F. and Parrish, R.S., 1988, "Developing joint probability distributions of soil water retention characteristics," *Water Resources Research*, 24:755-769.

Fredlund, D.G. and Xing, A., 1994, "Equations for the soil-water characteristic curve," *Canadian Geotechnical Journal*, Vol. 31, pp. 521-532.

Gee, G.W., Ward, A.L., Zhang, Z.F., Campbell, G.S., and Mathison, J., 2002, "The influence of hydraulic nonequilibrium on pressure plate data," *Vadose Zone Journal*, 1:172-178.

Kosugi, K., Hopmans, J.W., and Dane, J.H., 2002, "Parametric Models," In *Methods of Soil Analysis, Part 4, Physical Methods*, Soil Science Society of America, Book Series, No.5, Madison, WI.

Leij, F.J., Alves, W.J., van Genuchten, M.Th., and Williams, J.R., "The UNSODA unsaturated soil hydraulic database," *Res. Rep. 600 R-96 095*, USEPA, Cincinnati, OH.

Leong, E.C. and Rahardjo, H., 1997, "Reviews of soil-water characteristic curve equations," *Journal of Geotechnical and Geoenvironmental Engineering*, Vol. 123, pp. 1106-1117.

Lu, N. and Likos, W.J., 2004, *Unsaturated Soil Mechanics*, Wiley, New York, 556 pp.

Luckner, L., van Genuchten, M.Th., and Nielsen, D.R., 1989, "A consistent set of parametric models for the two-phase flow of immiscible fluids in the subsurface," *Water Resources Research*, 25: 2187-2193.

Mualem, Y., 1976, "A new model for predicting the hydraulic conductivity of unsaturated porous media," *Water Resources Research*, 12: 513-522.

Nimmo, J.R., 1991, "Comment on the treatment of residual water content in "A consistent set of parametric models for the two-phase flow of immiscible fluids in the subsurface" by L. Luckner *et al*., *Water Resources Research*, 27: 661-662.

Rawls, W.J. and Brakensiek, D.L., 1985, "Prediction of soil water properties for hydrologic modeling," In E.Jones and T.J. Ward Eds., *Watershed Management in the Eighties*, ASCE, Denver, CO., pp. 293-299.

Revil, A. and Lu, N., 2013, "Unified water isotherms for clayey porous materials," *Water Resources Research*, 49: 5685-5699.

Schaap, M.G. and Leij, F.J., 1998, "Database-related accuracy and uncertainty of pedotransfer functions," *Soil Science*, 163: 765-779.

Schneider, M. and Goss, K.-U., 2012, "Prediction of water retention curves for dry soils from an established pedotransfer function: evaluation of the Webb model," *Water Resources Research*, 48, W06603.

Sillers, W.S., Fredlund, D.G., and Zakerzadeh, 2001, "Mathematical attributes of some soil-water characteristic curve models," *Geotechnical and Geological Engineering*, 19, pp. 243-283.

Vanapalli, S.K., Sillers, W.S., and Fredlund, M.D., 1998, "The meaning and relevance of residual state to unsaturated soils," *Proc. 51st Canadian Geotechnical Conference*, Edmonton, Alberta, October 4-7.

van Genuchten, M.T., 1980, "A closed form equation for predicting the hydraulic conductivity of unsaturated soils," *Soil Science Society of America Journal*, Vol. 44, 892-898.

van Genuchten, M. Th., Leij, F.J., and Yates, S.R., 1991, "The RETC code for quantifying the hydraulic functions of unsaturated soils," *U.S. Department of Agriculture, Agricultural Research Service, Report IAG-DW12933934*, Riverside, CA.

van Genuchten, M., Leij, F., and Lund, L. (eds.), 1992, "Indirect methods for estimating the hydraulic properties of unsaturated soils," University of California, Riverside and US Department of Agriculture Salinity Laboratory, Riverside, CA, 718 p.

Vereecken, H., Weynants, M., Javaux, M., Pachepsky, Y., Schaap, M.G., and van Genuchten, M.Th., 2010, "Using pedotransfer functions to estimate the van Genuchten-Mualem soil hydraulic properties: a review," *Vadose Zone Journal*, 9:795-820.

Webb, S.W.D., 2000, "A simple extension of two-phase characteristic curves to include the dry region," Water Resour. Res., 36(6): 1425-1430.

Wösten, J.H.M., Pachepsky, Y.A., and Rawls, W.J., 2001, "Pedotransfer functions: bridging the gap between available basic soil data and missing soil hydraulic characteristics," *J. Hydrol*., 251: 123-150.

Yang, H., Rahardjo, H., Leong, E., and Fredlund, D., 1994, "Factors affecting drying and wetting soil-water characteristic curves of sandy soils, *Canadian Geotechnical J*., 41, 908–920.

Zapata, C.E., Houston, W.N., Houston, S.L., and Walsh, K.D., 2000, “Soil-water characteristic curve variability,” In *Advances in Unsaturated Geotechnics,* ASCE, pp 84-124: doi: 10.1061/40510(287)7.

TABLES

Table 5-1. SWCC fitting parameters for 1024 Sand (Liej et al., 1996) with and without parameter constraints.

Constraint	α (kPa^{-1})	n	m	S_r
None	1.70	3.36	0.23	0.11
$m = 1\text{-}1/n$	1.13	2.10	0.52	0.15
$S_r = 0$	2.29	6.72	0.07	0.00
$m = 1\text{-}1/n$; $S_r = 0$	1.39	1.62	0.38	0.00

FIGURES

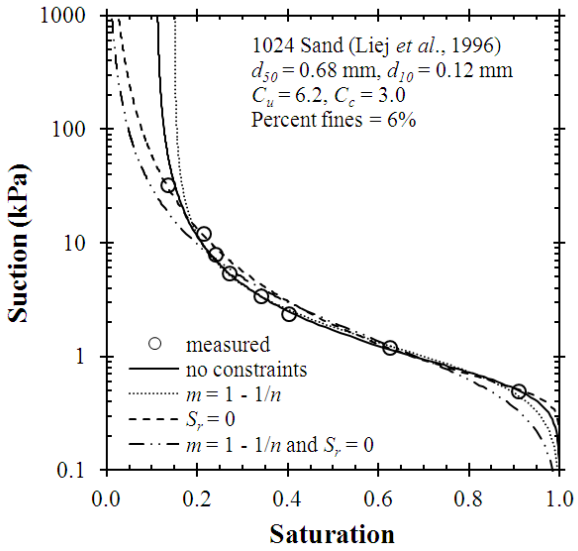

Figure 5-1. SWCC of typical sand and corresponding van Genuchten (1980) model for cases with and without applying parameter constraints.

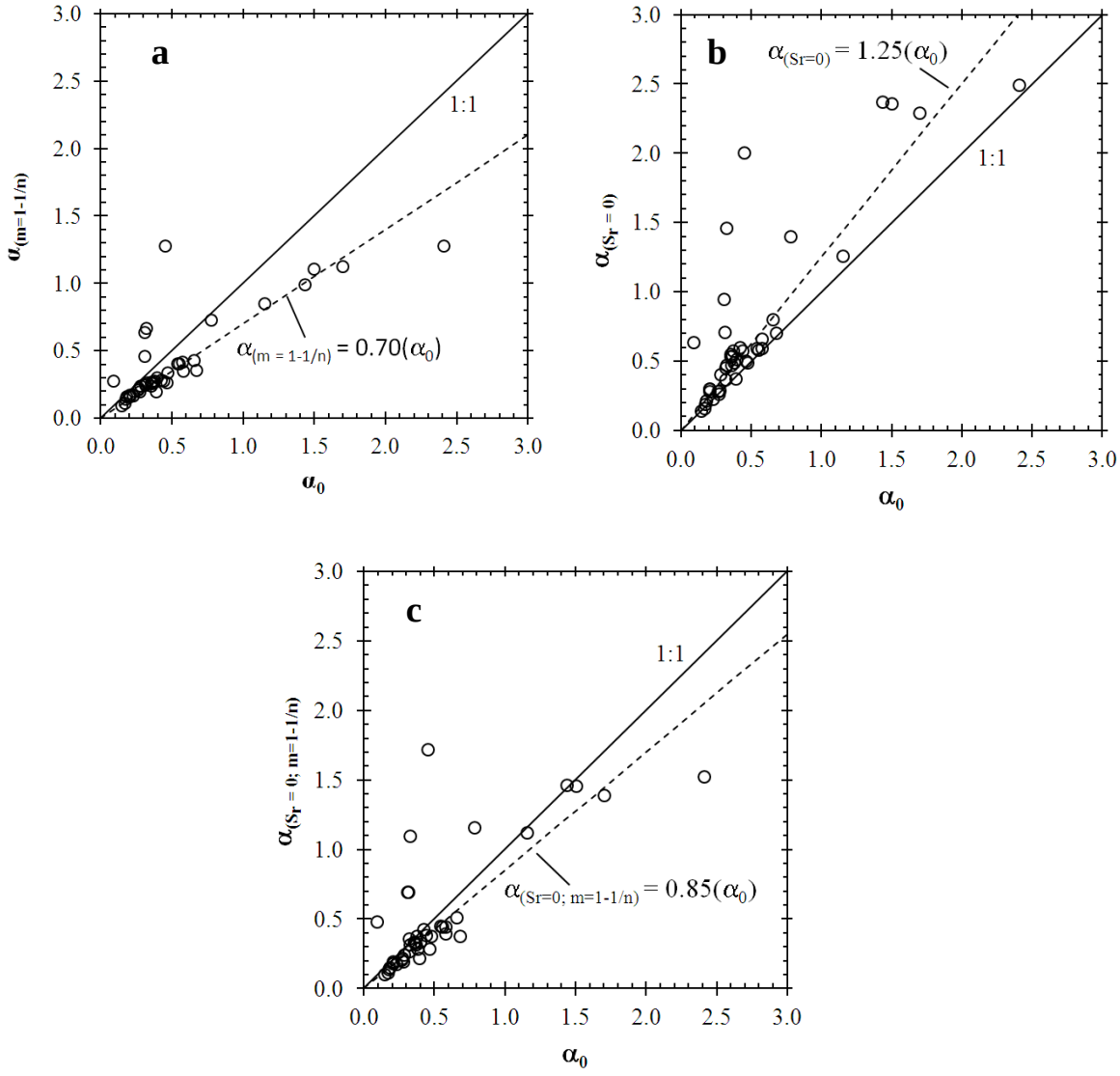

Figure 5-2. Influence of constraints on the van Genuchten (1980) α parameter for 44 sandy soils: (a) comparison of α obtained under no constraints and m = 1-1/n; (b) comparison of α obtained under no constraints and S_r = 0; (c) comparison of α obtained under no constraints and m = 1-1/n and S_r = 0.

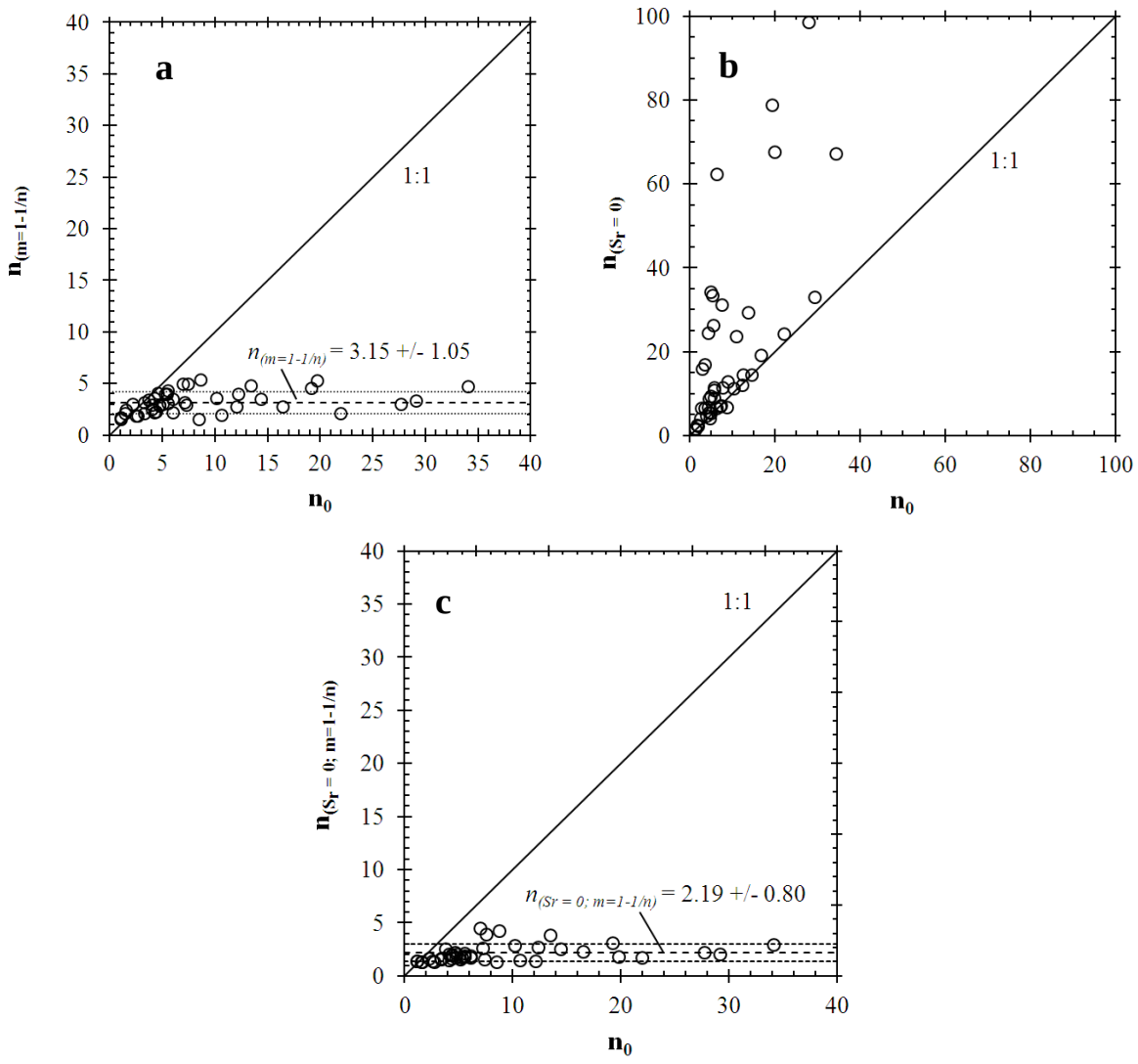

Figure 5-3. Influence of constraints on the van Genuchten (1980) *n* parameter for 44 sandy soils: (a) comparison of *n* obtained under no constraints and *m* = 1-1/*n*; (b) comparison of *n* obtained under no constraints and S_r = 0; (c) comparison of *n* obtained under no constraints and *m* = 1-1/*n* and S_r = 0.

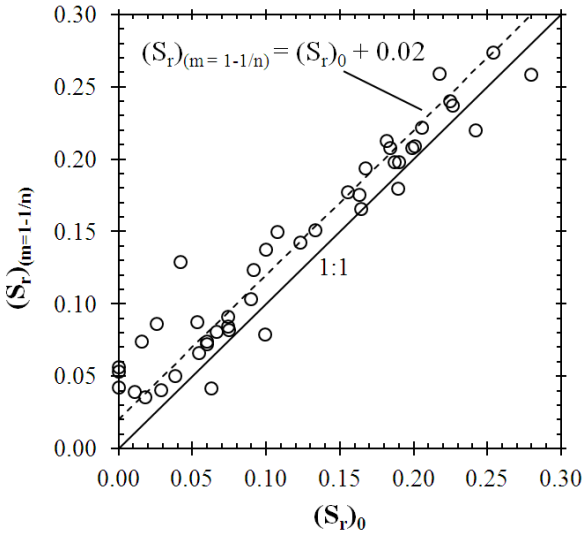

Figure 5-4. Influence of the $m = 1 - 1/n$ constraint on the van Genuchten (1980) S_r parameter.

CHAPTER SIX

APPENDIX-B

THERMAL RESISTIVITY DRY-OUT CURVES USING THREE LABORATORY METHODS AND THERMAL CONDUCTIVITY DRY-OUT CURVES COUPLED WITH SOIL WATER CHARATERISTIC CURVES USING MOFIFIED HANGING COLUMN METHOD FOR THIRTEEN SANDS

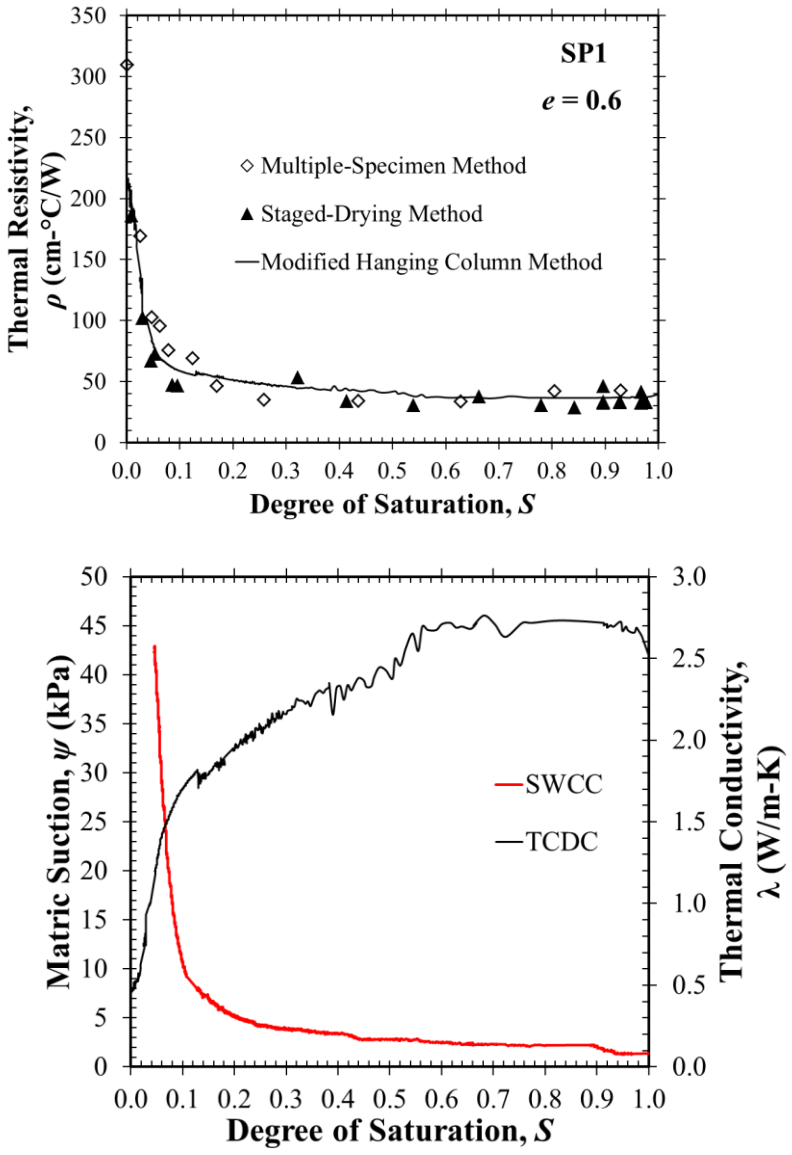

Figure 6-1. SP1 test results: (a) TRDCs using three methods; (b) TCDC coupled with SWCC

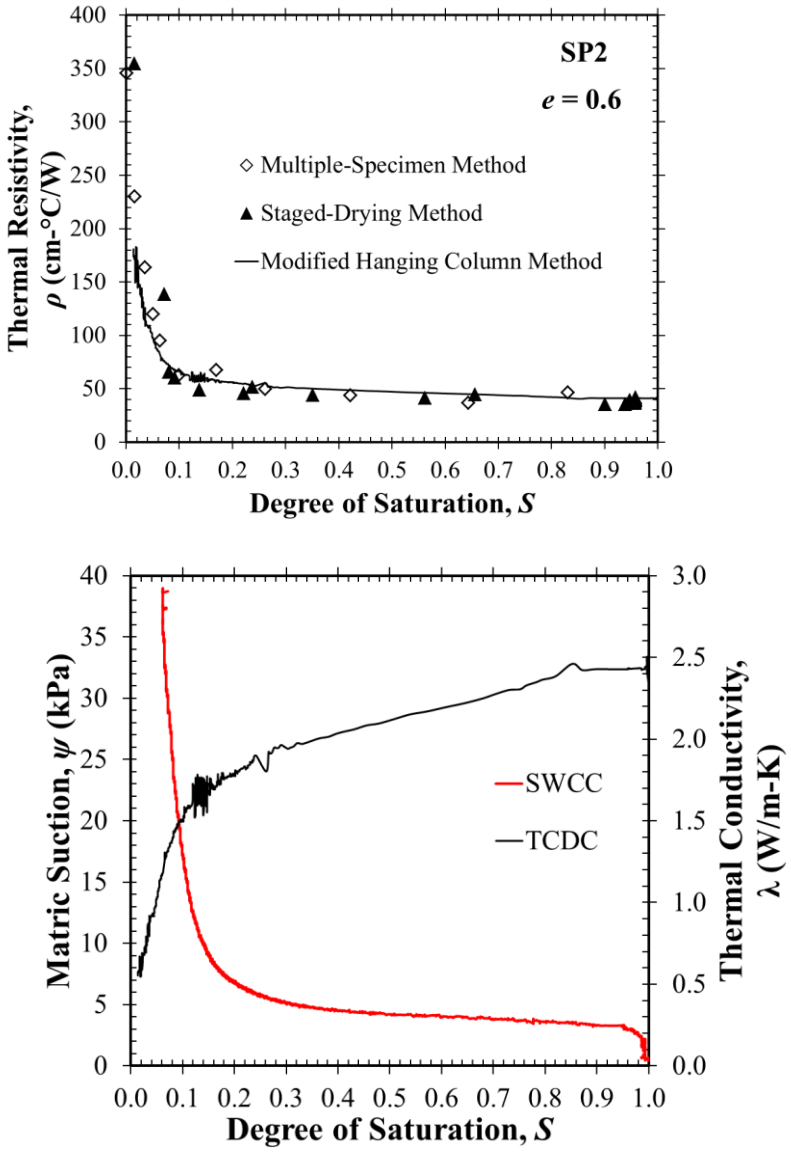

Figure 6-2. SP2 test results: (a) TRDCs using three methods; (b) TCDC coupled with SWCC

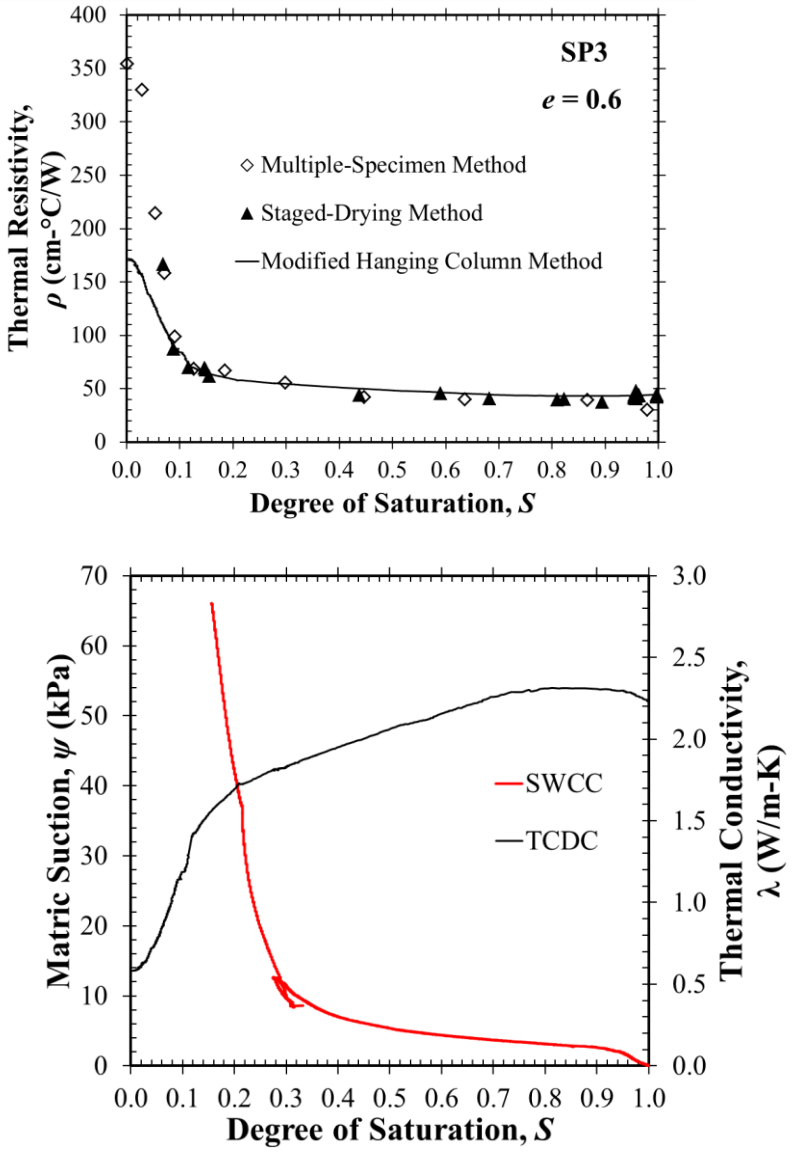

Figure 6-3. SP3 test results: (a) TRDCs using three methods; (b) TCDC coupled with SWCC

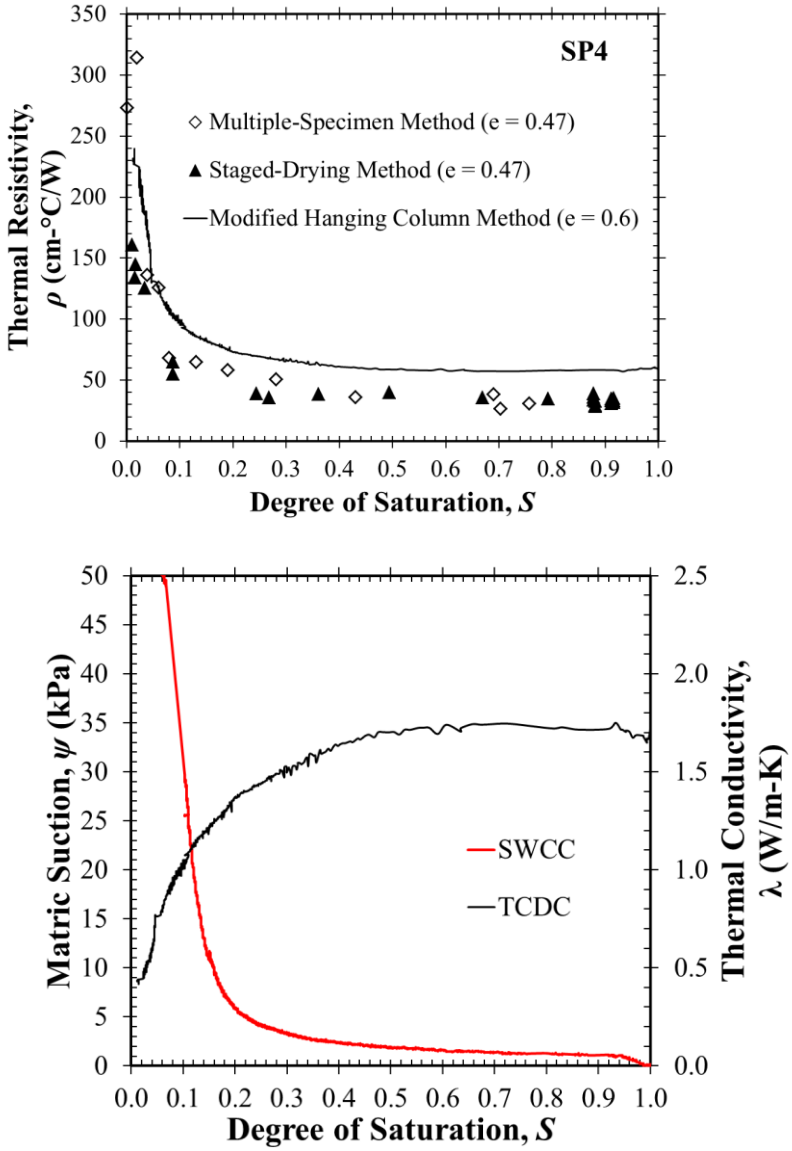

Note: The void ratios for SP4 were different for three test methods. Therefore, SP4 was removed for method comparison.

Figure 6-4. SP4 test results: (a) TRDCs using three methods; (b) TCDC coupled with SWCC

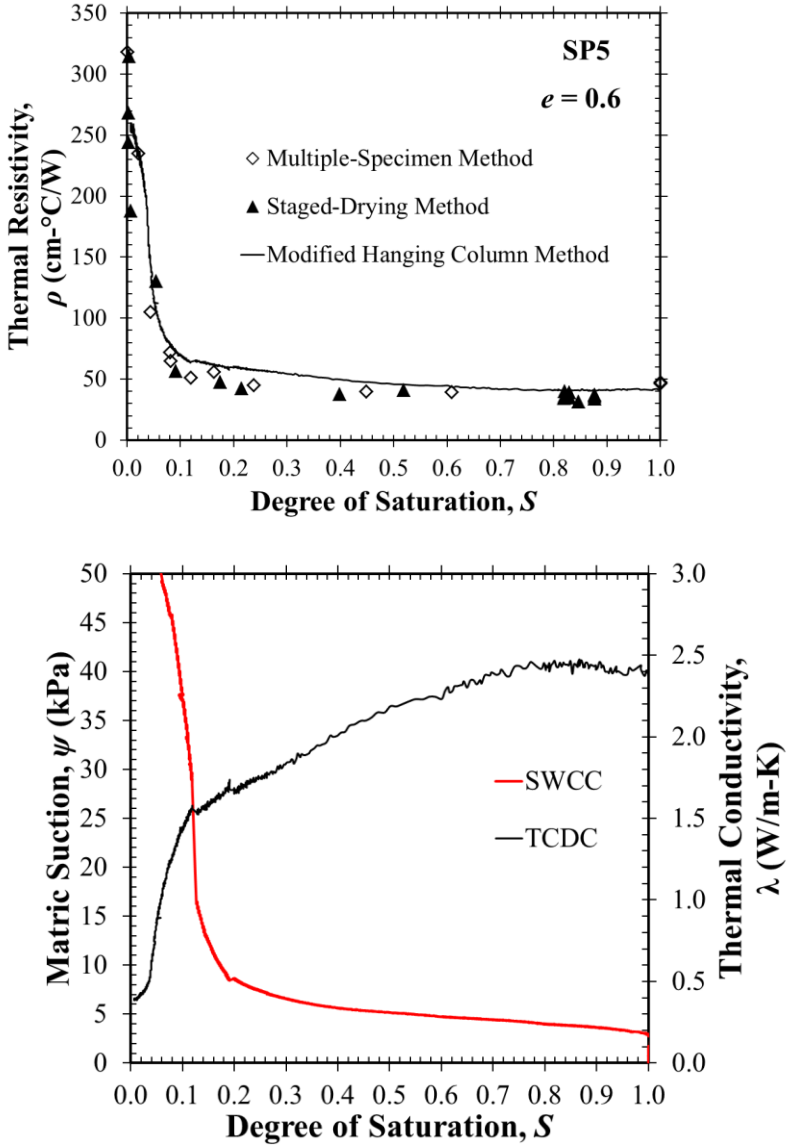

Figure 6-5. SP5 test results: (a) TRDCs using three methods; (b) TCDC coupled with SWCC

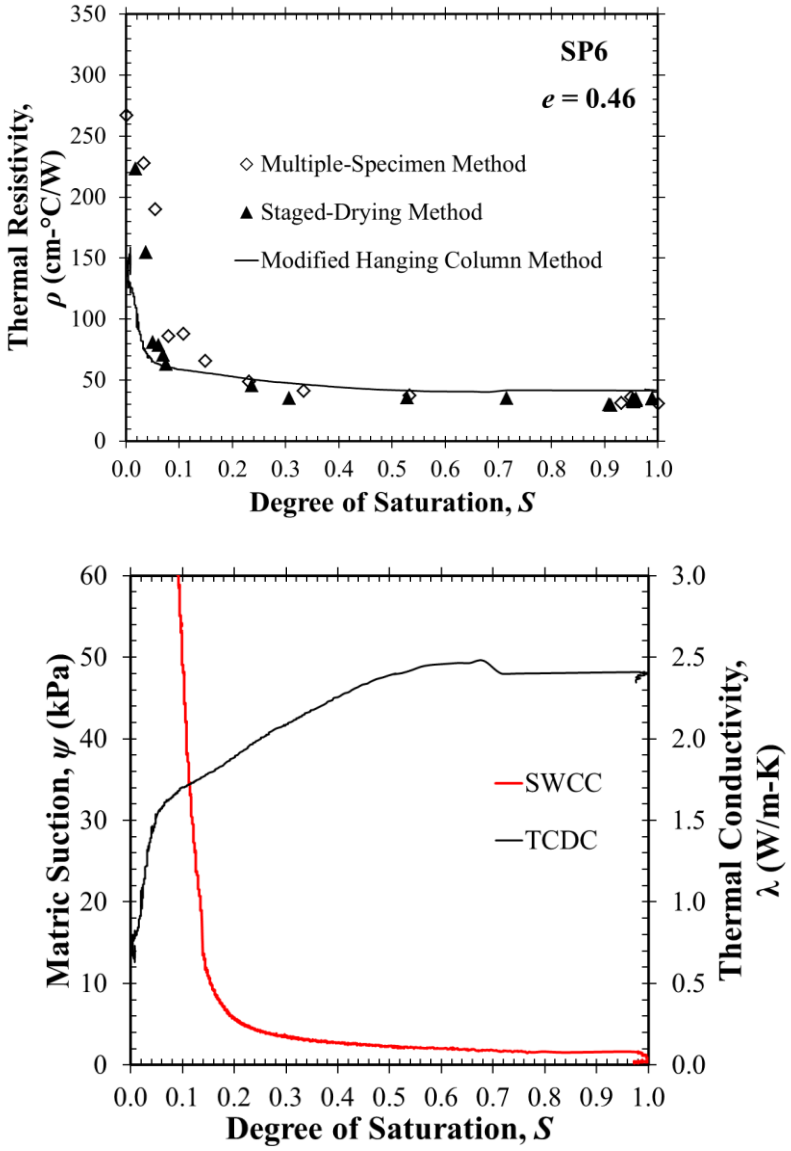

Figure 6-6. SP6 test results: (a) TRDCs using three methods; (b) TCDC coupled with SWCC

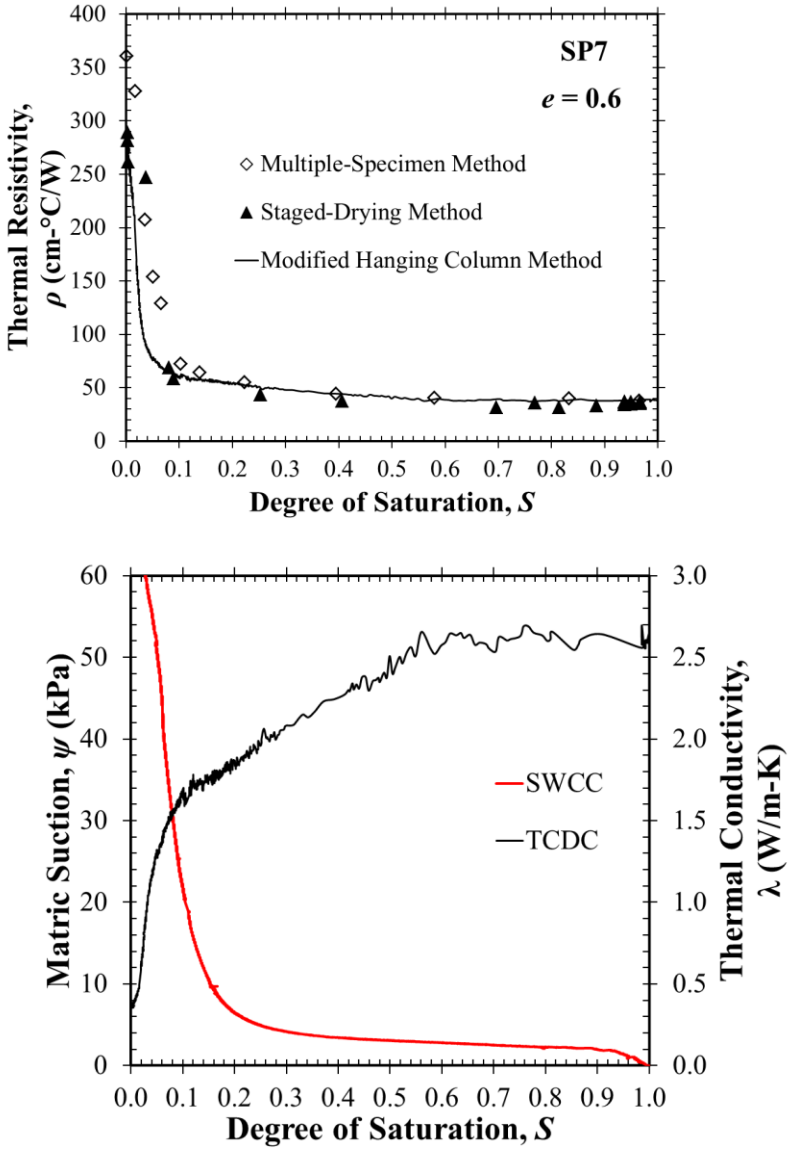

Figure 6-7. SP7 test results: (a) TRDCs using three methods; (b) TCDC coupled with SWCC

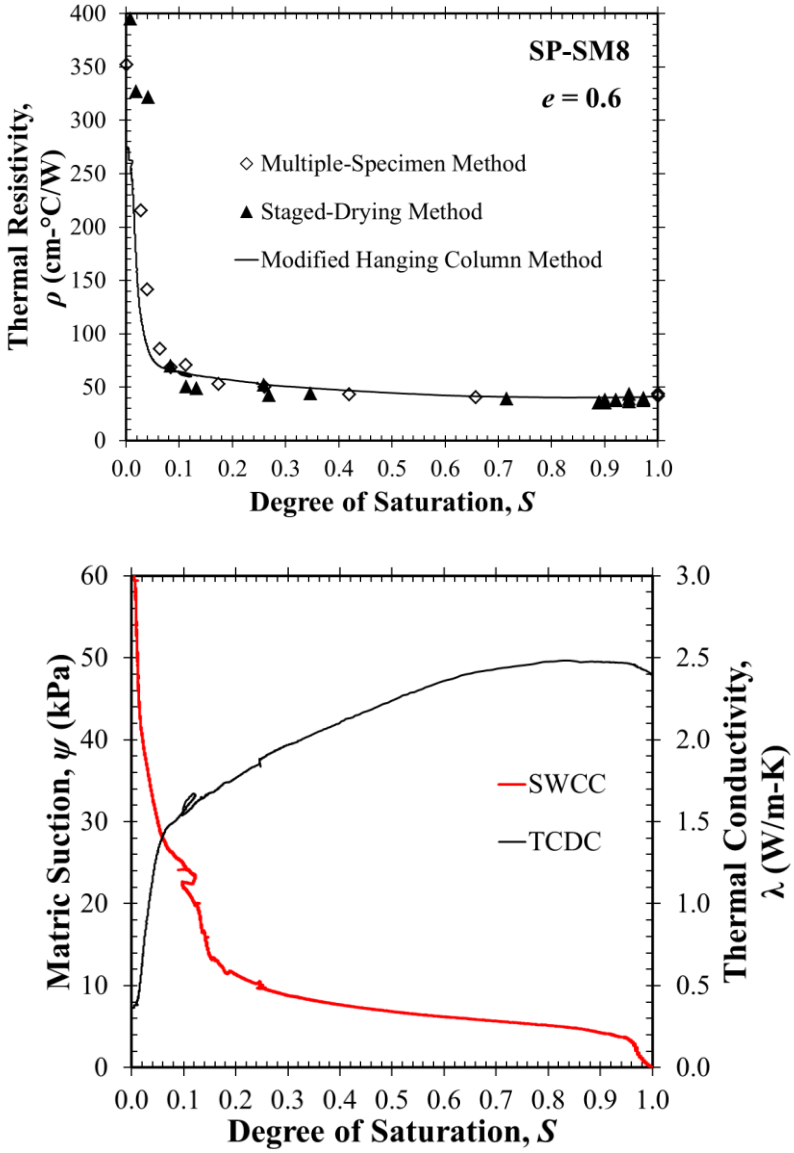

Figure 6-8. SP-SM8 test results: (a) TRDCs using three methods; (b) TCDC coupled with SWCC

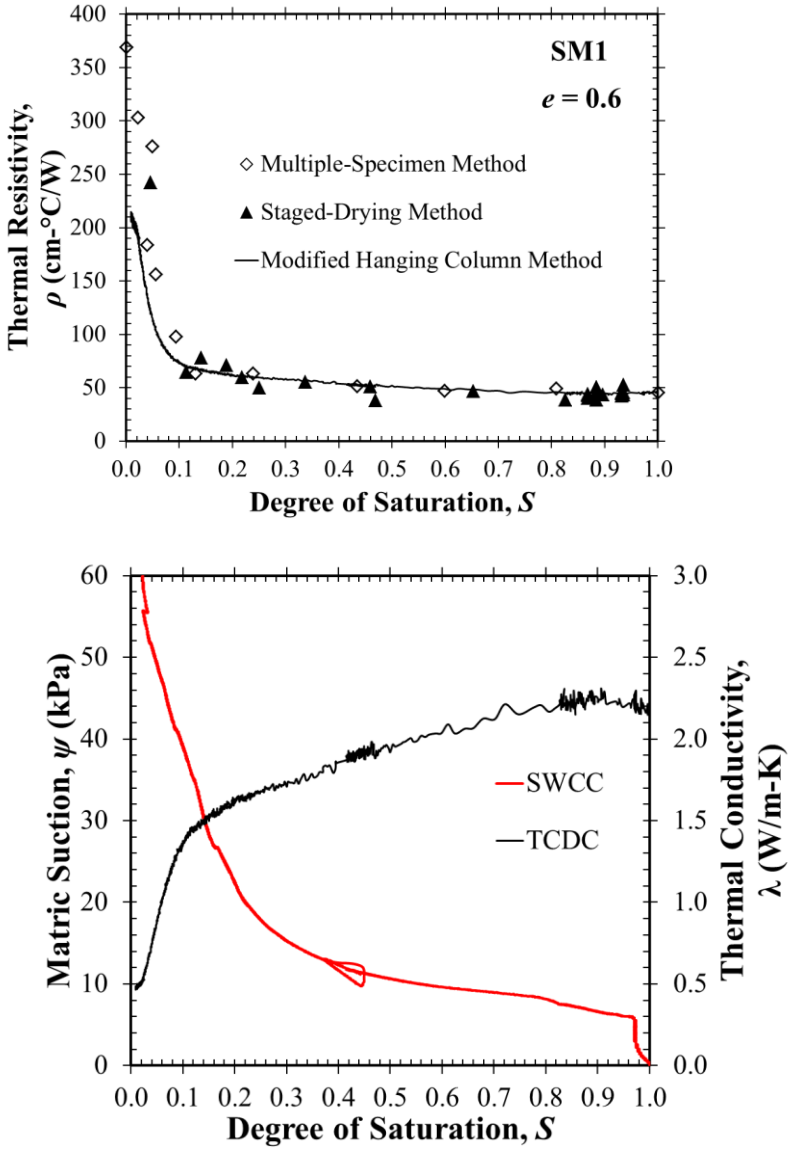

Figure 6-9. SM1 test results: (a) TRDCs using three methods; (b) TCDC coupled with SWCC

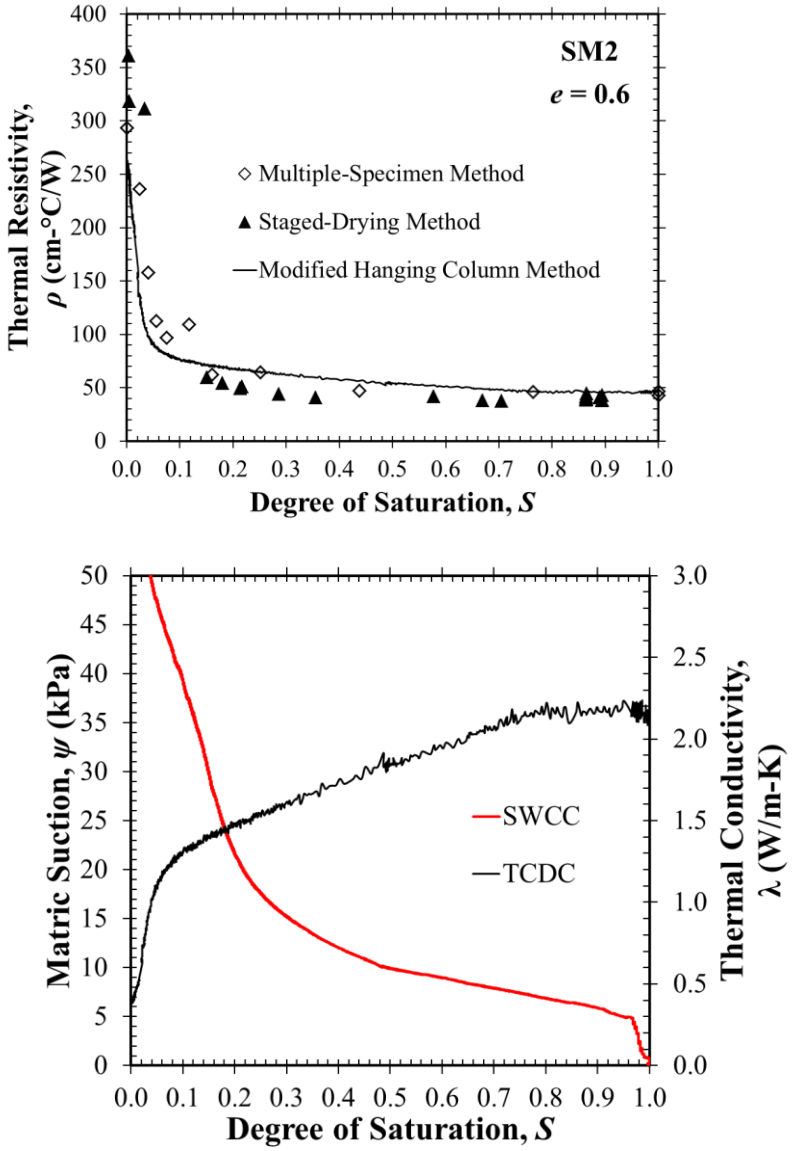

Figure 6-10. SM2 test results: (a) TRDCs using three methods; (b) TCDC coupled with SWCC

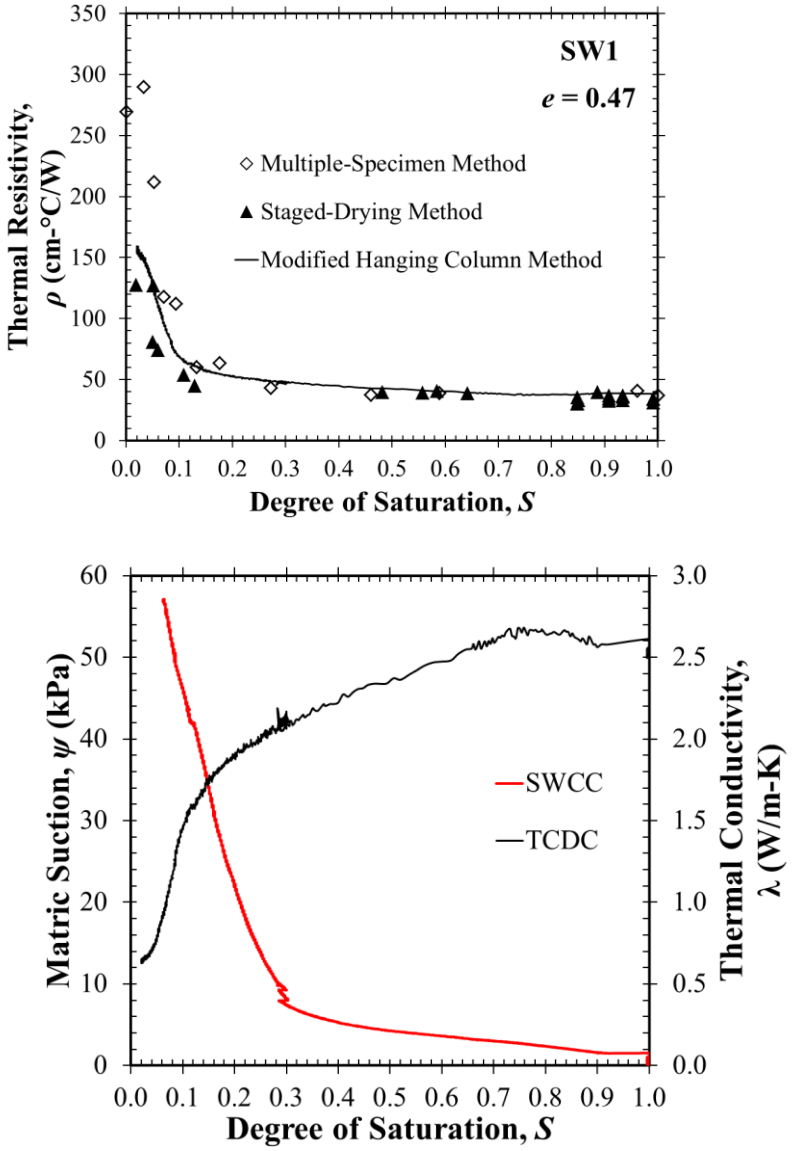

Figure 6-11. SW1 test results: (a) TRDCs using three methods; (b) TCDC coupled with SWCC

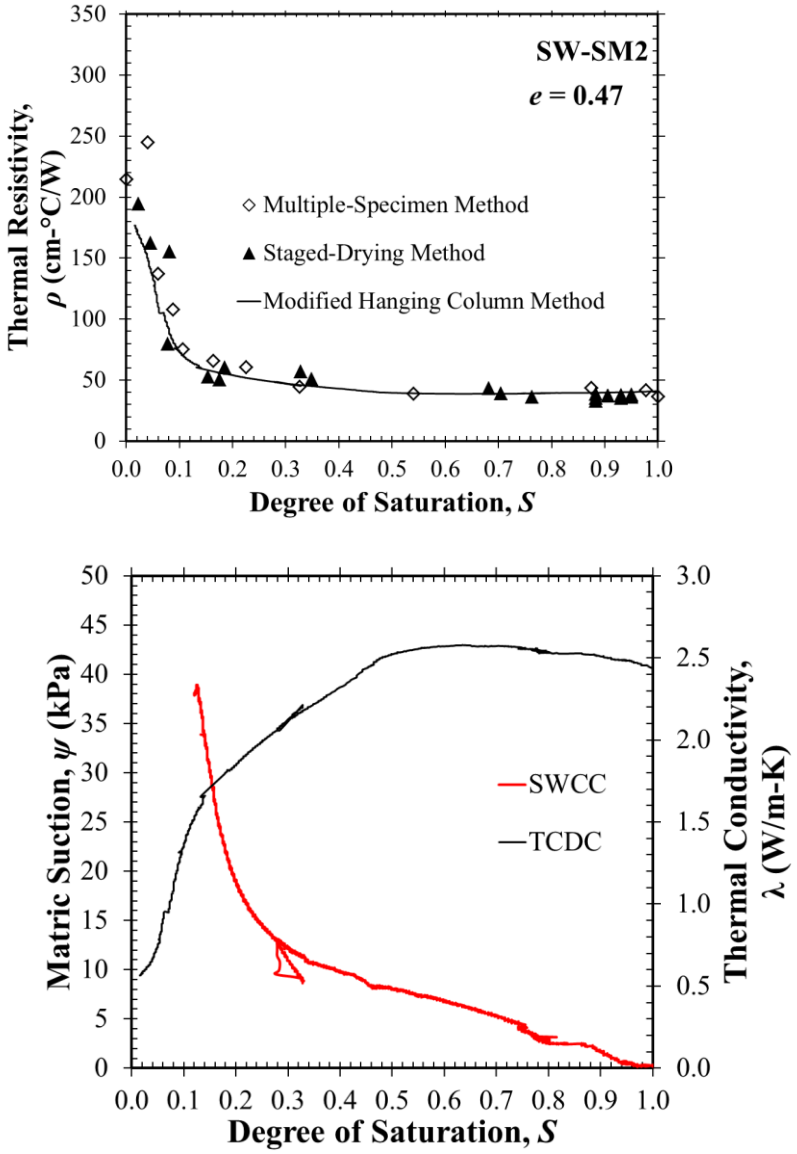

Figure 6-12. SW-SM2 test results: (a) TRDCs using three methods; (b) TCDC coupled with SWCC

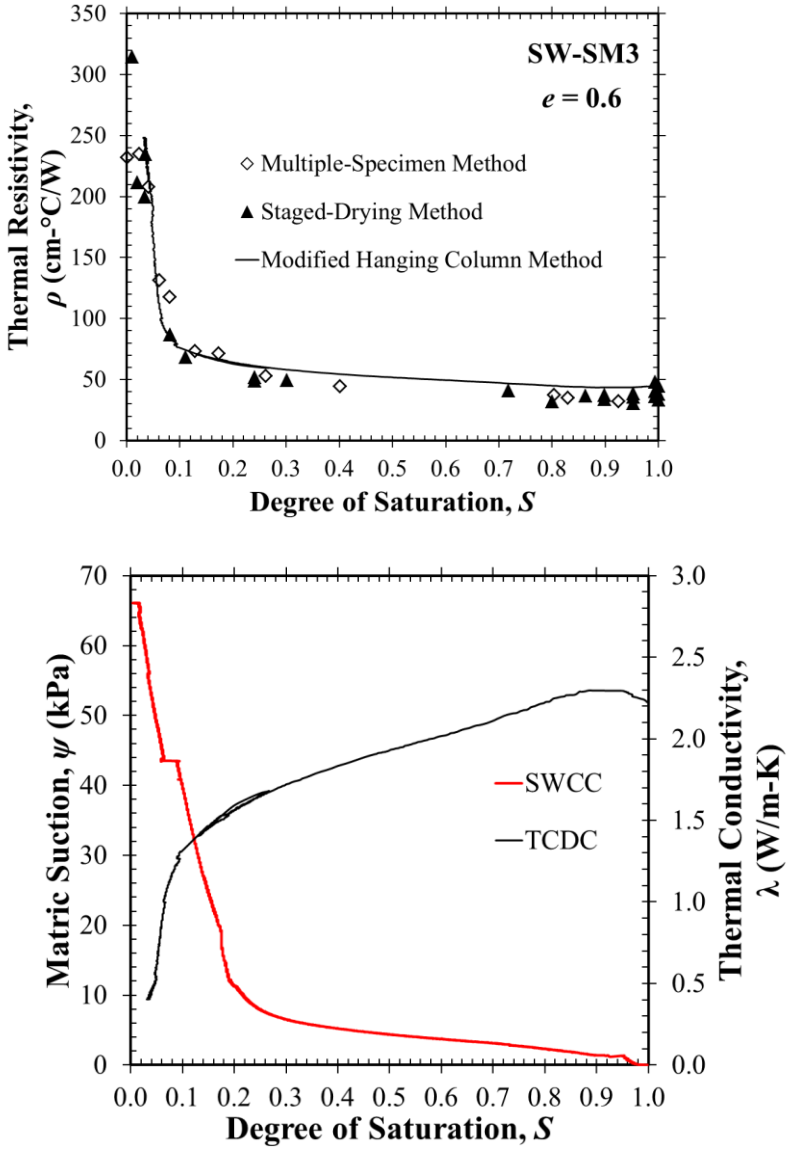

Figure 6-13. SW-SM3 test results: (a) TRDCs using three methods; (b) TCDC coupled with SWCC